

Institutionen för systemteknik

Department of Electrical Engineering

Examensarbete

Crank Angle Based Virtual Cylinder Pressure Sensor in Heavy-Duty Engine Application

Master's thesis performed in Vehicular Systems
at Linköping University
by

Mikael Gustafsson

LiTH-ISY-EX--15/4921--SE

Linköping 2015



Linköpings universitet
TEKNISKA HÖGSKOLAN

Crank Angle Based Virtual Cylinder Pressure Sensor in Heavy-Duty Engine Application

Master's thesis performed in Vehicular Systems
at Linköping University
by

Mikael Gustafsson

LiTH-ISY-EX--15/4921--SE


Supervisor: **Dr. Daniel Jung**
ISY, Linköping University

Dr. Ola Stenlås
SCANIA CV AB

Dr. Soheil Salehpour
SCANIA CV AB

Examiner: **Associate Professor Erik Frisk**
ISY, Linköping University

Linköping, 21 december 2015

	Avdelning, Institution Division, Department Division of Vehicular Systems Department of Electrical Engineering SE-581 83 Linköping	Datum Date 2015-12-21
Språk Language <input type="checkbox"/> Svenska/Swedish <input checked="" type="checkbox"/> Engelska/English <input type="checkbox"/> _____	Rapporttyp Report category <input type="checkbox"/> Licentiatavhandling <input checked="" type="checkbox"/> Examensarbete <input type="checkbox"/> C-uppsats <input type="checkbox"/> D-uppsats <input type="checkbox"/> Övrig rapport <input type="checkbox"/> _____	ISBN _____ ISRN LiTH-ISY-EX--15/4921--SE Serietitel och serienummer ISSN Title of series, numbering _____
URL för elektronisk version http://urn.kb.se/resolve?urn=urn:nbn:se:liu:diva-123710		
Titel Title Författare Author	Skattning av cylindertryck utifrån vevinkelshastighet Crank Angle Based Virtual Cylinder Pressure Sensor in Heavy-Duty Engine Application Mikael Gustafsson	
Sammanfattning Abstract <p>The in-cylinder pressure is an important signal that gives information about the combustion process. To further improve engine performance, this information can be used as a feedback signal in a control system. Usually a pressure sensor is mounted in the cylinder to extract this information. A drawback with pressure sensors is that they are expensive and have issues with aging. This master's thesis investigates the possibility to create a virtual sensor to estimate in-cylinder pressure based on crank angle degree sensor (CAD-sensor) data and physical models of the heavy-duty engine.</p> <p>Instead of using the standard mounted CAD-sensor an optical high-precision sensor measures the elapsed time between equidistant angles. Based on this signal the instantaneous angular acceleration was estimated. Together with the inertia of the crankshaft, connecting rods and pistons, an estimation of the engine torque was calculated. To be able to extract in-cylinder pressure from the estimated torque, knowledge about how the in-cylinder pressure signal propagates in the drivetrain to accelerate the flywheel needs to be known. Two engine models based on the torque balance on the crankshaft are presented. The fundamental difference between them is how the crankshaft is modeled, rigid body or spring-mass-damper system. The latter captures torsional effects of the crankshaft. Comparisons between the estimated torque from sensor data and the two engine models are presented. It is found that torsional effects of the crankshaft is present at normal engine speeds and has a significant influence on the flywheel torque.</p> <p>A separation of the gas torque contribution from one cylinder is done with CAD-sensor data together with the rigid body engine model. The in-cylinder pressure is then estimated by using the inverse crank-slider function and a Kalman filter estimator. The estimated pressure captures part of the compression and most of the expansion at engine speeds below 1200 RPM. Due to the crank-slider geometry the pressure signal disappears at TDC. The torsional effects perturb the estimated pressure during the gas exchange cycle.</p> <p>Further development must be made if this method is to be used on heavy-duty applications in the future.</p>		
Nyckelord Keywords CLCC, in-cylinder pressure, cylinder separation, torsion.		

Abstract

The in-cylinder pressure is an important signal that gives information about the combustion process. To further improve engine performance, this information can be used as a feedback signal in a control system. Usually a pressure sensor is mounted in the cylinder to extract this information. A drawback with pressure sensors is that they are expensive and have issues with aging. This master's thesis investigates the possibility to create a virtual sensor to estimate in-cylinder pressure based on crank angle degree sensor (CAD-sensor) data and physical models of the heavy-duty engine.

Instead of using the standard mounted CAD-sensor an optical high-precision sensor measures the elapsed time between equidistant angles. Based on this signal the instantaneous angular acceleration was estimated. Together with the inertia of the crankshaft, connecting rods and pistons, an estimation of the engine torque was calculated. To be able to extract in-cylinder pressure from the estimated torque, knowledge about how the in-cylinder pressure signal propagates in the drivetrain to accelerate the flywheel needs to be known. Two engine models based on the torque balance on the crankshaft are presented. The fundamental difference between them is how the crankshaft is modeled, rigid body or spring-mass-damper system. The latter captures torsional effects of the crankshaft. Comparisons between the estimated torque from sensor data and the two engine models are presented. It is found that torsional effects of the crankshaft is present at normal engine speeds and has a significant influence on the flywheel torque.

A separation of the gas torque contribution from one cylinder is done with CAD-sensor data together with the rigid body engine model. The in-cylinder pressure is then estimated by using the inverse crank-slider function and a Kalman filter estimator. The estimated pressure captures part of the compression and most of the expansion at engine speeds below 1200 RPM. Due to the crank-slider geometry the pressure signal disappears at TDC. The torsional effects perturb the estimated pressure during the gas exchange cycle.

Further development must be made if this method is to be used on heavy-duty applications in the future.

Acknowledgments

First of all, I would like to thank my supervisor Ola Stenlåås at Scania CV for all the support and guidance. Without your help I would not have come this far. Also I would like to thank Soheil Salehpour for your advice and discussions regarding signal processing. I would like to thank everyone at Engine Combustion Control Software for a great time, especially Stephan Zentner for all the laughs at the coffee breaks. A special thanks to Erik Frisk och Daniel Jung at Linköping University for always having time for questions and for giving me interesting ideas.

A big thank you to my parents Lars-Erik and Susanne for all your support during my time at the university. Finally, I would like to thank my girlfriend Sisi for always being there for me.

*Södertälje, December 2015
Mikael Gustafsson*

Contents

Notation	ix
1 Introduction	1
1.1 Background	1
1.2 Problem formulation	3
1.3 Delimitations	3
1.4 Method	4
1.4.1 Flywheel acceleration to in-cylinder pressure	4
1.4.2 CAD to crankshaft torque	4
1.4.3 Cylinder separation and pressure estimate	4
1.5 Outline	4
2 Engine Torque	7
2.1 Engine basics	7
2.1.1 Four-stroke	7
2.1.2 Crank-slider mechanism	9
2.1.3 CAD-sensor	10
2.1.4 Auxiliary units	11
2.2 Torque balancing equation	13
2.2.1 Mass torque	13
2.2.2 Friction Torque	15
2.2.3 Load Torque	16
2.2.4 Auxiliary torque	16
2.3 Crankshaft as a rigid body	16
2.4 Crankshaft dynamics	17
2.4.1 State-space model	19
2.5 Cylinder separation	19
3 Experimental setup	23
3.1 System overview	23
3.2 Experimental procedure	25
3.2.1 Data collected	26

4	Torque modeling	27
4.1	Friction models	27
4.1.1	Dynamic crankshaft friction input	29
4.2	Auxiliary models	29
4.2.1	Drive belt side	29
4.2.2	Transmission side	30
4.2.3	Fan	31
4.2.4	Dynamic crankshaft auxiliary inputs	32
4.3	Estimated torque from CAD-data	32
4.3.1	Filtering the CAD-signal	32
4.3.2	Torque estimation from CAD-signal	34
4.4	Engine simulations	34
4.4.1	Rigid body crankshaft	34
4.4.2	Dynamic crankshaft	35
5	Results and discussion	37
5.1	Comparison between T_{CAD} and T_{rbm}	37
5.1.1	Discussion	39
5.1.2	Conclusion rigid body	41
5.2	Comparison between T_{CAD} and T_{dcm}	42
5.2.1	Discussion	42
5.2.2	Conclusion dynamic crankshaft	43
5.3	Cylinder separation using rigid body model	45
5.4	Pressure estimation	47
5.4.1	Inverse crank slider	47
5.5	Kalman filter pressure estimation	49
6	Conclusions	53
	Bibliography	55

Notation

Variable	Description
A_p	Piston cross section area
C	Damper constant
E	Energy
GR	Gear ratio
I	Current
J	Moment of inertia
K	Spring constant
MEP	Mean effective pressure
T	Torque (subscript indicates from the source)
U	Voltage
V_D	Displaced volume per cycle
l	Connecting rod length
m	Mass
n_{cyl}	Number of cylinders
n_{eng}	Engine speed
n_r	Number of crank revolutions per engine cycle
p	In-cylinder pressure
r	Crankshaft radius
t_s	Sampling time
v	Speed
x^T	State vector
η	Efficiency
$\bar{\omega}$	Mean crankshaft angular speed
θ	Crank angle degree
$\dot{\theta}$	Crankshaft angular speed
$\ddot{\theta}$	Crankshaft angular acceleration
$\frac{ds(\theta)}{d\theta}$	Piston velocity with respect to CAD
$\frac{d^2s(\theta)}{d\theta^2}$	Piston acceleration with respect to CAD

Abbreviation	Description
BDC	Bottom Dead Center
CAD	Crank Angle Degree
CI	Compression Ignition
CLCC	Closed-Loop Combustion Control
ECU	Engine Control Unit
FFT	Fast Fourier Transform
LTI	Linear Time-Invariant
MEP	Mean Effective Pressure
MISO	Multiple-Input Single-Output
RPM	Revolutions Per Minute
SISO	Single-Input Single-Output
SOC	Start Of Combustion
SOI	Start of Injection
TDC	Top Dead Center
VS	Virtual Sensor

1

Introduction

1.1 Background

Today the automotive industry aims to reduce fuel consumption and emissions while keeping a good driveability. All things mentioned depend heavily on what goes on in the cylinders inside the engine during the combustion phase. When it comes to compression-ignited (CI) engines the combustion relies on the auto-ignition process. To further improve engine performance from the current open-loop control strategy, closed-loop combustion control (CLCC) might be needed [1, 2, 3].

With the use of the open-loop strategy, each cylinder has got cycle-to-cycle and cylinder-to-cylinder variations in mechanical work and emissions. These variations are due to that the in-cylinder pressure varies both in magnitude and timing relative to the crank angle degree (CAD) during the combustion.

To optimize delivered performance from the engine it is important that the pressure occurs at the right time so the lever from the crankshaft generates maximum torque. By using estimated combustion parameters, calculated from in-cylinder pressure, as a feedback signal it is possible to reduce these cycle-to-cycle and cylinder-to-cylinder variations.

Another benefit from using CLCC is that it can make small adjustments to the injection strategy to handle the different qualities of the fuel used. The diesel will differ slightly from the one used when mapping the engine. Fuel quality will for instance affect the ignition delay (time from start of injection (SOI) to start of combustion (SOC)). By adjusting the timing of injection the engine will increase its efficiency. There are many other advantages using CLCC [4, 5]; lower emissions, higher comfort and diagnostics on engine components - to mention a

few.

The most convenient way to estimate in-cylinder pressure is to mount pressure sensors in each cylinder of the engine. From the estimated pressure curve standard methods of estimating combustion parameters can then be used. Since the sensors are exposed to the harsh environment inside the cylinder they have to be durable. The sensors also need to deliver an accurate measurement of the pressure. As a consequence, these pressure sensors are expensive and usually not mounted on an engine as standard.

Other ways of estimating in-cylinder pressure have been investigated using torque sensors mounted on the crankshaft [6, 7], and engine speed variations measured on the flywheel [8, 9]. Another interesting approach to estimate individual cylinder pressure has been proposed in [10, 11, 12] using sliding-mode observers.

Some of the articles above use the standard mounted sensor that register the crank angle degree (CAD). A benefit of designing a combustion parameter estimator using this sensor, is that no additional sensors are required.

Cylinder pressure to CAD acceleration can be seen as a multiple-input single-output (MISO) system. Each cylinder will be an input that is superimposed via the crankshaft and affects the output, the acceleration of the CAD $\ddot{\theta}$. In addition to the torque produced by the pressure difference on the pistons T_{gas} , the crankshaft acceleration will be affected by other torques. For instance torque from friction T_{fric} within the engine, mass torque T_{mass} due to movement of pistons and connecting rods, torque needed to drive auxiliaries T_{aux} , and the load torque T_{load} from the driveline connected to the flywheel. Also the inertia of the crankshaft J_{cs} affects $\ddot{\theta}$.

$$J_{cs}\ddot{\theta} = T_{gas} + T_{fric} + T_{mass} + T_{aux} + T_{load} \quad (1.1)$$

In this equation the crankshaft is assumed to be a rigid body.

To calculate the gas torque from Eq. (1.1) models of the other torques mentioned above needs to be derived. Since the gas torque depends on contributions from all the cylinders the next step is to estimate the gas torque $T_{gas,i}$ contribution of each cylinder from $T_{gas} = \sum_{i=1}^{nCyl} T_{gas,i}$. This process will be called cylinder separation.

At higher engine speeds torsional effects might occur in the crankshaft and affects the torque signal. Then a model of the crankshaft is needed to perform the cylinder separation. This has been done in [13] by using the inverse of the Fourier transform derived from physical modeling. With some assumptions the cylinder separation method makes the MISO system into several single-input single-output (SISO).

With the torque contribution from one cylinder known the in-cylinder pressure can be calculated using the geometry of the crank-slider mechanism.

Once the pressure has been extracted from the CAD-signal, combustion param-

ters can be estimated using thermodynamic laws. Heat release analysis is a procedure that uses cylinder pressure to calculate the rate at which heat is released in the combustion chamber [14]. The heat release position and shape is of special interest when it comes to CLCC.

Another approach to estimate in-cylinder pressure is proposed in [15]. Here the CAD-signal is used together with measured in-cylinder pressure from one cylinder. The measured cylinder pressure is then used as an initial estimate for the rest of the cylinders together with a dynamic crankshaft model and simulated. The initial induced gas torque is then corrected based on the difference between the measured and simulated crank angle position by using an optimal signal tracking algorithm. The algorithm is a standard linear quadratic problem.

1.2 Problem formulation

The goal of this thesis is to estimate the in-cylinder pressure using a virtual sensor (VS), based on the crankshaft angular velocity measured at the flywheel on a heavy-duty engine. By deriving models of the different torques affecting the crankshaft acceleration in Eq. (1.1), a cylinder separation can be performed to estimate the gas torque of a single cylinder. The proposed method in [13] will be used. A difference from their work will be that the angular acceleration of the crankshaft is used instead of torque measurements. To achieve this:

- Models from in-cylinder pressure to acceleration of the flywheel needs to be derived. By using these physical models the inverse calculation from the CAD-signal to pressure can later be performed.
- Models of other torques affecting the crankshaft is needed.
- The estimated in-cylinder pressure calculated by the VS will be compared with measurements from in-cylinder pressure data.

1.3 Delimitations

This section is used as a reference to limit the scope of the thesis.

- The reference engine in this project is an inline 6-cylinder engine. This type of engine will be used in the test bench when collecting data. Other models of engines is not investigated in this thesis.
- The estimator does not need to work online. The designed estimator will be implemented in Matlab/Simulink using sampled data to estimate in-cylinder pressure offline.
- Since there are many engine modes in the engine management system, this thesis will only focus on one fuel injection strategy when estimating the pressure. Apart from the main injection a pilot injection may be used. Strategies with several pilot and post injections will not be investigated.

- This thesis will not estimate combustion parameters.
- Only sampled data from static working points will be used for model design.

1.4 Method

The estimator of in-cylinder pressure will be implemented in Matlab/Simulink. The subsections below describes a preliminary approach to reach the thesis goal.

1.4.1 Flywheel acceleration to in-cylinder pressure

Before the VS will be designed an understanding of how the in-cylinder pressure affects the flywheel needs to be known. Physical models of e.g. the crank slider mechanism and crankshaft dynamics will then be inversed so the in-cylinder pressure can be estimated from the flywheel acceleration.

1.4.2 CAD to crankshaft torque

To get the CAD acceleration the first approach will be to take the derivative of the known sampled CAD-signal. Some signal processing may be needed if the CAD-signal is perturbed. With an estimation of the crankshafts acceleration, Newton's second law for rotation will be used to estimate the total torque on the crankshaft. To perform this step the inertia of the crankshaft needs to be known.

1.4.3 Cylinder separation and pressure estimate

With an estimate of the total crankshaft torque it is time to perform the cylinder separation. This step will get the individual cylinder torque contribution. The approach here is to use the cylinder separation proposed in [13]. The torque-to-pressure inversion is then performed by analyzing the geometry of the crank-slider mechanism.

1.5 Outline

The first chapter introduces the background and problem formulation to this thesis. Also some of the related work done in this area are presented. In chapter two the fundamental theory needed to understand the process within an engine and the engines auxiliary units are given. To model the engine as a complete system the torque balancing equation is introduced to show how each sub-system affects the rotational acceleration. The torque balancing equation is described in two ways depending on if the crankshaft is modeled as a rigid body or flexible. The third chapter describes the experimental part where the data used throughout this thesis was collected. Chapter four gives the friction and auxiliary models. The signal processing of the CAD-sensor data is described. The engine is also simulated with two different crankshaft models to generate torque traces over an engine cycle. The results are presented in chapter five. Comparisons are made

with estimated torque traces from CAD-sensor data with the two crankshaft models. Using the rigid-body crankshaft model and torque trace from CAD-sensor data an estimation of the gas torque is calculated. Finally an estimation of the cylinder pressure using a Kalman filter is presented.

2

Engine Torque

2.1 Engine basics

This section aims to go through the fundamental parts, geometry and important parameters of a reciprocating engine. In Figure 2.1 a Scania 6-cylinder inline engine is shown which is similar to the one used throughout this thesis.

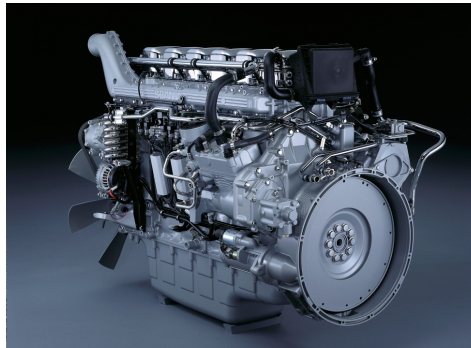


Figure 2.1: Scania DC1307 engine. (Reproduced with permission from Scania).

2.1.1 Four-stroke

Today most reciprocating engines operates according to the four-stroke cycle. The four strokes are related to the piston movement inside the cylinder and a stroke refers to a full movement of the piston, end-to-end, inside the cylinder. The complete four-stroke process form a single thermodynamic cycle from which mechan-

ical work will be extracted. When the piston has completed its four strokes the crankshaft has turned two revolutions, which is also known as an engine cycle.

The positions when the piston is farthest from, or closest to, the crankshaft are known as the top dead center (TDC) and bottom dead center (BDC). Dead center is any position when the connecting rod and crankshaft align. The four-stroke process explained below is for a CI engine.

Intake (TDC-BDC): During the intake stroke the intake valve is open and as the piston is moving downwards the cylinder gets filled with air from the intake manifold. The intake valve closes just before the piston reaches BDC.

Compression (BDC-TDC): The newly air-filled cylinder starts the compression stroke. The air temperature and pressure increases as the piston moves upwards due to the mechanical work done on the air charge. The fuel injection from the rail starts some crank angle degrees before the piston reaches the TDC. In CI engines, fuel is directly injected into the combustion chamber. The injected fuel auto-ignites due to the high pressure and temperature of the air charge before TDC is reached. The combustion phase continues to the expansion stroke.

Expansion (TDC-BDC): The combustion continues and finishes approximately 40° after TDC. Positive torque is produced on the crankshaft, via the crank-slider mechanism, as long as the in-cylinder pressure is greater than the pressure inside the engine block. Before the piston reaches BDC the exhaust valve opens, appr. 140° after TDC. Because the pressure inside the cylinder is greater than in the exhaust manifold, exhaust gases start rushing out through the exhaust port.

Exhaust (BDC-TDC): The gas inside the cylinder gets pushed out through the exhaust port. When the exhaust valve closes near TDC the in-cylinder pressure is close to the pressure inside the exhaust system. Then the four-stroke process starts over.

The four-stroke cycle is shown in Figure 2.2.

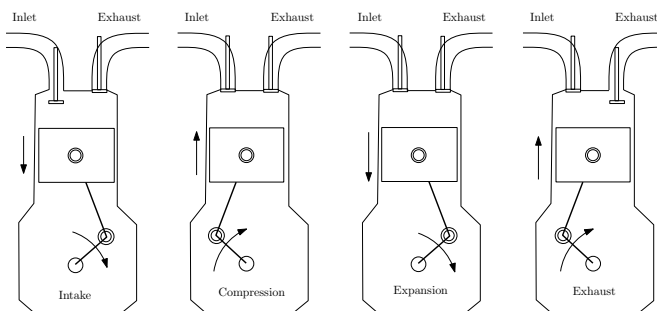


Figure 2.2: Different strokes of a four-stroke engine.

2.1.2 Crank-slider mechanism

This section will describe how the in-cylinder pressure generates torque via the crank-slider mechanism. A basic outline of the crank-slider geometry, for one cylinder, with relevant parts is shown in Figure 2.3.

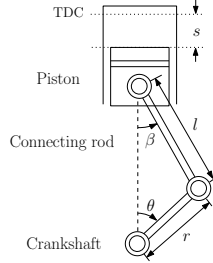


Figure 2.3: Crank-slider geometry.

The equations below are found in [16]. The torque generated from the pressure difference on the pistons via the crank-slider mechanism to the crankshaft will be referred to as the gas torque.

$$T_{gas,i}(\theta) = (p(\theta) - p_0) \cdot A_p \frac{ds(\theta)}{d\theta} \quad (2.1)$$

In Eq. (2.1) the gas torque contribution on the crankshaft is from a single cylinder. The equation is derived from indicated specific work. Here the pressure inside the cylinder is a function of the crank angle $p(\theta)$. The crankcase pressure is assumed to be constant p_0 , sometimes set to the ambient atmospheric pressure. A_p is the piston cross section area. The distance from TDC to the piston head, referred to as piston stroke or piston displacement $s(\theta)$, is derived from the geometry of the crank-slider mechanism, see Figure 2.3.

$$s(\theta) = r \left(1 - \cos \theta + \frac{l}{r} \left(1 - \sqrt{1 - \frac{r^2}{l^2} \sin^2 \theta} \right) \right) \quad (2.2)$$

In Eq. (2.2) l is the connecting rod length and r the crank radius. The gas torque in Eq. (2.1) depends on the derivative of piston stroke with respect to crank angle θ , piston velocity in the crank angle domain, see Eq. (2.3).

$$\frac{ds(\theta)}{d\theta} = r \left(\sin \theta + \frac{r}{l} \cdot \frac{\sin \theta \cos \theta}{\sqrt{1 - \frac{r^2}{l^2} \sin^2 \theta}} \right) \quad (2.3)$$

Later, when calculating the mass torque, the second derivative of the piston

stroke with respect to crank angle is needed, see Eq. (2.4).

$$\frac{d^2s(\theta)}{d\theta^2} = r \left(\cos \theta + \frac{\frac{r}{l}(\cos^2 \theta - \sin^2 \theta) + \frac{r^2}{l^2} \sin^4 \theta}{\left(\sqrt{1 - \frac{r^2}{l^2} \sin^2 \theta}\right)^3} \right) \quad (2.4)$$

The derivation of Eq. (2.1)-(2.4) can be found in [16]. An alternative derivation of the gas torque is found in [17].

In Eq. (2.1) the torque contribution of one cylinder is calculated. This thesis will focus on a 6-cylinder engine where the angle between adjacent firing cylinders is 120° and the firing order is 1,5,3,6,2,4.

With $\theta_{TDC,i} = \{0^\circ, 480^\circ, 240^\circ, 600^\circ, 120^\circ, 360^\circ\}$ defined as the crank angle in which the i th cylinder is in its TDC position, the angle of the i th cylinder, as defined in Figure 2.3, becomes $\theta_i = \theta - \theta_{TDC,i}$.

2.1.3 CAD-sensor

At the end of the crankshaft the flywheel is mounted. Around the flywheel radial holes are drilled as shown in Figure 2.4. The holes are drilled with an equidistant angle of 6° . The standard mounted sensor used here are of inductive type, it registers when a hole passes by detecting changes in the magnetic field. The time difference between two holes are measured with high accuracy and since the sensor signal is synchronous with the CAD the crankshaft rotational speed can be calculated. Two holes are omitted on the flywheel so the sensor can easily register when the engine has turned one revolution.

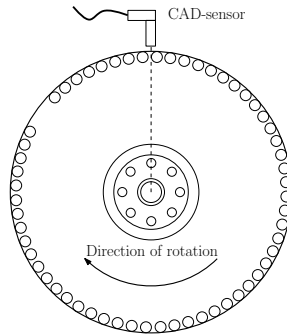


Figure 2.4: Flywheel and CAD-sensor. The flywheel has radial holes drilled on the outside of the flywheel.

Apart from the standard mounted sensor described above an optical high precision sensor was used during the experiments conducted in the test bench. A specially developed marker disk is mounted on the flywheel. The disc has got holes with an equidistant angle of 0.5° drilled into it. The optical sensor head is fixed to the engine block. This type of sensor is too expensive to be a standard

mounted sensor in a production engine. Also since it is of optical type it is sensitive to dirt, which the inductive sensor is not. Data from the high precision sensor was used throughout this thesis.

The measured CAD-sensor data from the test bench must be differentiated to get the CAD acceleration $\ddot{\theta}$. Before this can be done the measured data needs to be low-pass filtered due to noise in the signal. Details of how the filtering was done on the CAD-sensor data is found in Section 4.3 together with how the estimated total torque was calculated.

2.1.4 Auxiliary units

Several auxiliary units are mounted on the engine. Some of these units are vital for the engine to operate correctly while others are needed for the vehicle. All of the units are connected and driven by the crankshaft. This is done in three different ways, via a driving belt in the front side of the engine, by the transmission found behind the flywheel and lastly the fan is connected with a viscous coupling mounted on the extension of the crankshaft on the front side of the engine. This means that some of the mechanical work produced by the engine will be consumed by these systems and affect the output torque to the rest of the driveline.

This section will list the different auxiliary components found on a Scania DC13 engine. The list below considers the auxiliary systems that are connected to the drive belt in the front end of the engine.

Alternator: The alternator converts mechanical energy to electrical energy and is used to charge the battery and to power the electrical systems while the engine is running. The torque needed to drive the alternator will oscillate during one revolution but can be approximated as constant for a given operating point. This constant depends on rotational speed of the alternator and the current output from it.

AC-compressor: The ac-compressor, or pump, increase the pressure of the refrigerant vapor in the air conditioning system. The mechanical work performed on the refrigerant will in the end make a more pleasant environment for the driver in the cabin. The pump is of piston type and the torque needed to drive the ac-compressor varies over a cycle of the compressor when it is engaged. But in comparison with other auxiliary units the torque needed is small and is assumed to be constant.

Coolant pump: To be able to remove heat from the engine a cooling system is needed. This system removes heat by recirculating a coolant through the engine block and through the radiator where the liquid exchange heat to the atmosphere. The coolant pump increases the flow rate of the liquid and thus increase the heat transfer. The coolant pump is of centrifugal type and the torque needed to drive it depends on the rotational speed of the pump.

On the other side of the engine, behind the flywheel, the transmission that drives the rest of the auxiliary units is found. The transmission consists of several cog-

wheels with different gearing. With the use of cogwheels there will be no slip which can occur on the drive belt side. The following list considers the auxiliary units connected to the transmission.

Oil pump: The oil pump circulates the engine oil and lubricates all the moving parts inside the engine and at the same time cools the engine by carrying heat away from the moving parts. The oil pump is of gear type.

Air compressor: Air brakes are used on heavy-duty trucks and buses. Also when a trailer is connected it must be linked to the brake system of the truck. The air compressor pressurizes a storage tank and when the brake pedal is pressed the compressed air is used to apply the brakes. The air compressor engages when the pressure in the storage tank is low. The compressor is of piston type and the torque needed will oscillate over a revolution of the axis.

Fuel pump: The fuel pump consists of two different pumps connected to the same axle. Firstly there is a low pressure pump that ensures that the fuel circuit has the fuel it needs. It delivers the fuel from the fuel tank to the rest of the system. This pump is of gear type. The "low" pressurized fuel arrives at the high pressure pump that increase the fuel pressure considerably and delivers the fuel to the common rail system. The high pressure pump is of piston type and the torque needed depends on the position of the pistons meaning it will fluctuate during a revolution of the axis.

Hydraulic pump: The hydraulic pump adds controlled energy to the power steering mechanism when the driver turns the steering wheel. The power steering helps considerably when the vehicle is at stand still and at slow speeds. Thus the torque used by the pump depends on the driving condition. This pump is of wing type.

Camshaft: The camshaft controls the opening and closing of the exhaust and inlet valves. The camshafts timing is of great importance and rotates exactly at half the crankshaft speed. The camshaft lobes pushes against push rods that in turn pushes down the valves. The springs on the valves returns them to the closed position and at the same time return some of the energy back on the camshaft via the push rod. This leads to variations in the torque needed to drive the crankshaft during an engine cycle.

As mentioned earlier the fan is connected to an extension of the crankshaft using a viscous coupling. The purpose of the fan is to cool the engine by increasing the air flow through the radiator and at the same time increasing the air flow around the engine. The torque needed to drive the fan depends on the state of the viscous coupling and the engine speed.

2.2 Torque balancing equation

Section 2.1.2 explained how the in-cylinder pressure affects the crankshaft. The gas torque is the only torque that delivers energy to the crankshaft in an internal combustion engine. To be able to extract the in-cylinder pressure/gas torque by using the CAD-sensor all other torques that affect the angular acceleration of the crankshaft $\ddot{\theta}$ needs to be modeled. The relationship between the net external torque and the angular acceleration is given by Newton's second law for rotation. For a single cylinder engine, as discussed in Section 2.1.2, the equation becomes

$$0 = T_{gas}(\theta) - T_{mass}(\theta, \dot{\theta}, \ddot{\theta}) - T_{fric}(\theta) - T_{load}(\theta) - T_{aux}. \quad (2.5)$$

The equation is often referred to as the torque balancing equation [6, 16]. Here, T_{mass} is the mass torque due to acceleration of masses in the crank-slider mechanism, T_{fric} is the friction torque, and T_{load} is the load torque. Also included in the equation is T_{aux} which is the torque needed to run the auxiliary systems on the engine. Usually this torque is included in the load torque but is here stated explicitly. The crankshaft inertia J_{cs} is included in the mass torque expression.

2.2.1 Mass torque

The inertia in a reciprocating engine depends on the crank angle due to the motion of the crank-slider mechanism masses, the pistons and connecting rods. The torque originating from this motion will be called mass torque. The mass torque has been derived from the kinetic energy of the engine masses in motion [16].

$$E_{mass} = \int_0^{2\pi} T_{mass} d\theta = \frac{1}{2} J \dot{\theta}^2 \quad (2.6)$$

The mass torque is then given by the derivative, with respect to θ , of Eq. (2.6) and results in the following equation.

$$T_{mass} = J\ddot{\theta} + \frac{1}{2} \frac{dJ}{d\theta} \dot{\theta}^2 \quad (2.7)$$

The first term in Eq. (2.7) represents the rotational masses and the other term the oscillating masses which have changing inertia with respect to the crank angle. The motion of the piston may be assumed as translational inside the cylinder and the motion of the crankshaft as rotational. The connecting rod undergoes both a translational and rotational motion and will be simplified. This is done by placing parts of the mass of the connecting rod in the oscillating mass and the rest in the rotating part and the end result will become a two mass system, see Figure 2.5.

With the center of gravity of the connecting rod known the oscillating mass be-

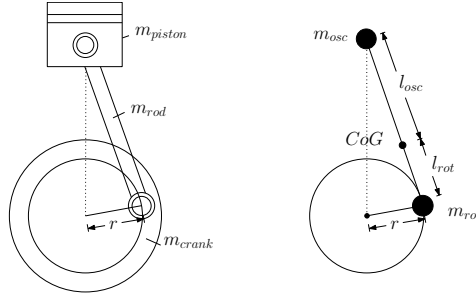


Figure 2.5: Two point mass system, dividing the connecting rod.

comes.

$$m_{osc} = m_{piston} + m_{rod} \frac{l_{osc}}{l} \quad (2.8)$$

The rotating mass consists of the mass of one crank lever together with the rotating mass of the connecting rod.

$$\frac{m_{rot}}{n_{cyl}} = \frac{m_{cs}}{n_{cyl}} + m_{rod} \frac{l_{rot}}{l} \quad (2.9)$$

Where n_{cyl} is the number of cylinders and m_{cs} is approximated from the moment of inertia of the crankshaft according to.

$$m_{cs} = \frac{J_{cs}}{r^2} \quad (2.10)$$

Here it is worth noting that the crankshaft inertia J_{cs} given on the left hand side in Eq. (2.5) is now included in the mass torque.

This two point mass approximation is known as the statically equivalent model [6]. Still the total mass and center of gravity is still the same as for the original body, but the splitting of the connecting rod mass changes the moment of inertia slightly. The statically equivalent model is sufficient when it comes to model the torsional effects in the crankshaft [6].

The kinetic energy of the two masses will then become.

$$E_{mass} = \frac{1}{2} \cdot \frac{m_{rot}}{n_{cyl}} \cdot v_{rot}^2 + \frac{1}{2} \cdot m_{osc} \cdot v_{osc}^2 \quad (2.11)$$

The time derivative of the kinetic energy is

$$\frac{dE_{mass}}{dt} = \frac{dE_{mass}}{d\theta} \cdot \frac{d\theta}{dt} = T_{mass} \cdot \dot{\theta} \quad (2.12)$$

The calculations of the time derivative are omitted, but the resulting mass torque

from the piston, connecting rod and crank throw becomes.

$$T_{mass,i}(\theta, \dot{\theta}, \ddot{\theta}) = \underbrace{\left(\underbrace{m_{osc} \cdot \left(\frac{ds_i}{d\theta} \right)^2}_{J_{osc}(\theta)} + \underbrace{\frac{m_{rot}}{n_{cyl}} \cdot r^2}_{J_{rot}} \right)}_{J(\theta)} \ddot{\theta} + \underbrace{\frac{1}{2} \left(2 \cdot m_{osc} \frac{ds_i}{d\theta} \cdot \frac{d^2s_i}{d\theta^2} \right)}_{\frac{dJ_{osc}(\theta)}{d\theta}} \dot{\theta}^2 \quad (2.13)$$

The derivation of Eq. (2.13) can be found in [16]. Here it is worth noting that the second term depends on engine speed squared, $\dot{\theta}^2$, and grows large at higher RPM.

Constant inertia and speed mass torque

Further some simplifications can be done to the mass torque in Eq. (2.13) [6]. The varying inertia part takes on values between zero and $m_{osc} \cdot r^2$ and can be approximated by its mean value.

$$J_{osc}(\theta) = m_{osc} \cdot \left(\frac{ds_i}{d\theta} \right)^2 \approx \bar{J}_{osc} = \frac{m_{osc}}{2} \cdot r^2 \quad (2.14)$$

The constant approximation can be done since it is only a small part of the total inertia of the crankshaft. Note that the simplification is only done in the first term of Eq. (2.13), otherwise the second term will become zero. Also the crankshaft rotational speed $\dot{\theta}$ can be approximated as constant $\bar{\omega}$ even though it varies during the revolution of the crankshaft. With these simplifications the mass torque then becomes

$$\bar{T}_{mass}(\theta, \bar{\omega}, \ddot{\theta}) = \left(\bar{J}_{osc} + \frac{m_{rot}}{n_{cyl}} \cdot r^2 \right) \ddot{\theta} + \frac{1}{2} \cdot \frac{dJ_{osc}(\theta)}{d\theta} \bar{\omega}^2. \quad (2.15)$$

This will be referred to as the constant inertia and speed mass torque. When a dynamic model of the crankshaft is used, this approximation of the mass torque will be used. The errors introduced with constant inertia and constant speed are studied in [6].

2.2.2 Friction Torque

The friction torque is here defined as the parasitic losses due to resistance to relative motion of moving parts within the engine, friction. By removing part by part on an engine and perform motored test with different engine speeds, the friction of each component can be estimated. The procedure is known as engine break down test [18]. Models of the friction of different components within the engine is found in Section 4.1.

2.2.3 Load Torque

In the test bench a dynamometer is connected to the flywheel of the engine which measures the torque output on the flywheel. In this thesis the measured torque from the dynamometer will be the load torque T_{load} .

2.2.4 Auxiliary torque

Models of all the auxiliary components listed in Section 2.1.4 is needed. Modeling a component is a very time consuming work and in this thesis models available within Scania is used. More details on this can be found in Section 4.2.

2.3 Crankshaft as a rigid body

When assuming the crankshaft to be stiff it can be modeled as a rigid body. The torque balancing equation can then be used.

$$J(\theta)\ddot{\theta} = T_{gas}(\theta) - f(\theta)\dot{\theta}^2 - T_{fric}(\theta) - T_{load}(\theta) - T_{aux} \quad (2.16)$$

In the equation above the gas torque $T_{gas}(\theta)$ will be the summed contribution from all cylinders. This makes it possible to write the total gas torque as.

$$T_{gas}(\theta) = \sum_{i=1}^6 (p(\theta_i) - p_0) \cdot A_p \cdot r \cdot \left(\sin \theta_i + \frac{r}{l} \cdot \frac{\sin \theta_i \cos \theta_i}{\sqrt{1 - \frac{r^2}{l^2} \sin^2 \theta_i}} \right) \quad (2.17)$$

The moment of inertia is the sum of all cylinders and depends on crank angle.

$$J(\theta) = \left(m_{rot} \cdot r^2 + m_{osc} \sum_{i=1}^{n_{cyl}} \left(\frac{ds_i}{d\theta} \right)^2 \right) \quad (2.18)$$

Also the oscillating part of the mass torque becomes a sum over the cylinders. The oscillating mass torque then becomes.

$$f(\theta)\dot{\theta}^2 = \frac{1}{2} \left(2 \cdot m_{osc} \sum_{i=1}^{n_{cyl}} \frac{ds_i}{d\theta} \cdot \frac{d^2s_i}{d\theta^2} \right) \dot{\theta}^2 \quad (2.19)$$

The rigid body approach is investigated to see if it is sufficient to model the engine. Due to its simplicity the calculations using this approach will not be so complex. The cylinder separation using this approach will be similar to the one described in Section 2.5, but without the dynamic models.

2.4 Crankshaft dynamics

During normal engine operation the crankshaft will be exposed to oscillatory torques that will twist parts of the crankshaft relative to other. This is due to the cyclic operation of the engine. The crankshaft has got resonate modes that are more or less excited by the combustions [13].

In this section a model of the crankshaft capable of describing these dynamic torsional effects is described. The crankshaft is modeled as rotating masses interconnected with linear springs and dampers, spring-mass-damper system, which is often used to model torsional effects in a crankshaft [6, 13, 19, 20]. The rotating masses are the damper wheel, crank-slider mechanisms and flywheel all which are assumed to be rigid bodies. These masses will be referred to as nodes. The axis connecting the nodes are modeled as parallel linear springs, $K_{i,i-1}$, and dampers, $C_{i,i-1}$, and will be called relative elements. The springs will store potential energy when twisted and together with the dampers model the torsional behavior in the crankshaft. This means that some of the gas torque contribution will be stored in the elements for a short period of time and will be released somewhat later, especially during the combustion when the gas torque magnitude is much bigger than any of the other torques affecting the crankshaft. As the combustion frequency gets closer to the resonate modes of the crankshaft it will have greater torsional effects.

The spring-mass-damper system is illustrated in Figure 2.6. The inertias J_i of each node needs to be known. The flywheel and damping wheel have constant inertias. The crank-slider mechanism for each cylinder has, as showed in Section 2.2.1, a angle-dependent inertia and is nonlinear. The simplification with constant inertia and constant speed, Eq. (2.15), will instead be used in the dynamic crankshaft case. The inertia for each cylinder node $i = 3..8$ will then be.

$$J_i = \bar{J}_{osc} + \frac{m_{rot}}{n_{cyl}} \cdot r^2 \quad (2.20)$$

This simplification is one step towards making the spring-mass-damper system linear.

Also seen are the dampers C_i connected between the nodes and a non-rotating frame. These dampers model the friction losses in the different bearings in the crankshaft system, and will be referred to as absolute elements.

As part of the design phase of the crankshaft, pistons and connecting rods the inertia and the constants of the relative springs and dampers are calculated [6].

In Figure 2.6 the external torques T_i are included. The torque from auxiliary systems connected to the drive belt in the front end of the engine will be an input on the front end mass T_2 . At the flywheel the load torque measured by the engine brake in the test cell are summed together with the torque from the auxiliary systems connected to the transmission side. In the case of torque input from each cylinder it is affected by three different torques, gas torque, mass torque

and piston friction. The mass torque input will be the second term in Eq. (2.15).

$$T_{p,i} = \frac{1}{2} \cdot \frac{dJ_{osc}(\theta)}{d\theta} \cdot \bar{\omega}^2 \quad (2.21)$$

The piston friction is small in comparison with gas and mass torque and will thus be assumed to be zero in this thesis work. The torque input of each cylinder then becomes.

$$T_i = T_{gas,i}(\theta) + T_{p,i}(\theta, \bar{\omega}) \quad (2.22)$$

The 6-cylinder engine will be modeled with nine masses. Each mass will have an angle θ_i and angle velocity $\dot{\theta}_i$. The motion equations for each rotating mass can be written as follows.

$$J_i \ddot{\theta}_i = C_{i+1,i}(\dot{\theta})_{i+1} - \dot{\theta}_i + K_{i+1,i}(\theta_{i+1} - \theta_i), \text{ for } i = 1 \quad (2.23)$$

$$J_i \ddot{\theta}_i = C_{i+1,i}(\dot{\theta})_{i+1} - \dot{\theta}_i - C_i \dot{\theta}_i + K_{i+1,i}(\theta_{i+1} - \theta_i) + T_i, \text{ for } i = 2..8 \quad (2.24)$$

$$J_i \ddot{\theta}_i = C_{i+1,i}(\dot{\theta})_{i+1} - \dot{\theta}_i - C_i \dot{\theta}_i + K_{i+1,i}(\theta_{i+1} - \theta_i) + T_{load}, \text{ for } i = 9 \quad (2.25)$$

With this multi-body extension the torque balancing equation may be expressed as

$$\mathbf{J} \ddot{\theta} + \mathbf{C} \dot{\theta} + \mathbf{K} \theta = \mathbf{T}_{gas}(\theta) + \mathbf{T}_{fric}(\theta) + \mathbf{T}_{load}(\theta) + \mathbf{T}_{mass}(\theta) \quad (2.26)$$

Here $\ddot{\theta}$, $\dot{\theta}$ and θ are column vectors with the dimension $[9 \times 1]$. The inertia matrix \mathbf{J} will be diagonal, the spring \mathbf{C} and damping \mathbf{K} matrix will have a 2×2 across the diagonal, tridiagonal, due to the interconnected springs and dampers. The dimensions of these matrices will be 9×9 . All torques will be column vectors that depends on the angle of the cylinder relative to the crankshaft.

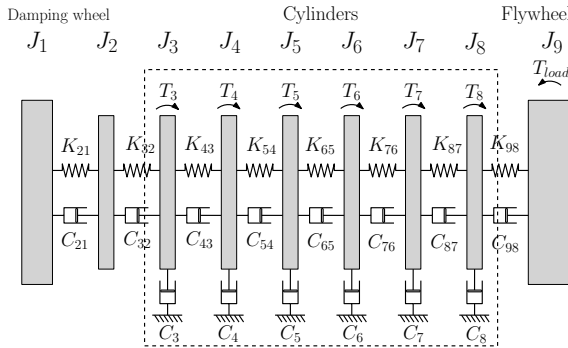


Figure 2.6: 9 DOF lumped torsional vibration model of a 6-cylinder engine.

2.4.1 State-space model

By introducing θ_i and $(\theta_i(t) - \theta_{i-1}(t))$ as states in Eq. (2.23)-(2.25) it is possible to write the dynamic crankshaft model in state-space form. The state vector will be of size 17×1 . This is the same approach as used in [19].

$$x^T = [\dot{\theta}_1, \dot{\theta}_2, \theta_2 - \theta_1, \dot{\theta}_3, \theta_3 - \theta_2, \dot{\theta}_4, \theta_4 - \theta_3, \dot{\theta}_5, \theta_5 - \theta_4, \dot{\theta}_6, \theta_6 - \theta_5, \dot{\theta}_7, \theta_7 - \theta_6, \dot{\theta}_8, \theta_8 - \theta_7, \dot{\theta}_9, \theta_9 - \theta_8] \quad (2.27)$$

If the angular positions of each inertia is used in the input torques the state-space equations will be nonlinear [19]. The state-space representation can be written as follows

$$\begin{aligned} \dot{x}(t) &= f(x(t), u(t)) \\ y(t) &= h(x(t), u(t)) \end{aligned} \quad (2.28)$$

Where $u(t)$ is the input torques to the crankshaft. By using the measured output from the flywheel $\dot{\theta}$ and using this as angular velocity to the input torques $u(t)$ the inputs will be independent of the states and can be calculated separately. This approximation make it to a continuous-time LTI state-space system

$$\begin{aligned} \dot{x}(t) &= Ax(t) + Bu(t) \\ y(t) &= \dot{\theta}_1(t) = [1, 0, \dots, 0]x(t) \end{aligned} \quad (2.29)$$

For further details the reader should look into [19].

2.5 Cylinder separation

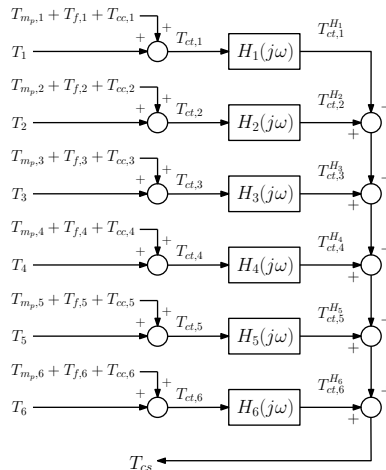


Figure 2.7: Crankshaft torque model with six parallel SISO systems of a 6-cylinder engine.

The process of estimating individual torque contributions of a firing cylinder from the angular acceleration will be referred to as cylinder separation. The method used here was first described in [13].

With a linear MISO crankshaft model it is possible to separate it to parallel transfer functions. By sending an impulse through the MISO system, on each input one at a time, the output becomes the impulse response h_i of the transfer function $H_i(j\omega)$ of each SISO system. The separation and the resulting parallel SISO systems are shown in Figure 2.7. The impulse response relates the torque input T_i from one cylinder via the crank throw to the crankshaft. The total torque the crankshaft is exposed to, from all the cylinders, then becomes.

$$T_{cs} = \sum_{i=1}^{n_{cyl}} h_i * T_i \quad (2.30)$$

Where $*$ denotes the convolution.

The system inversion method requires that only one input signal at a time is to be estimated, the other must be regarded as known. This means that only one cylinder is in its combustion phase at each time instance. A combustion starts at $\sim 5^\circ$ before TDC and finishes at $\sim 40^\circ$ after TDC. In figure 2.8a pressure traces for all six cylinders are shown. For cylinder three, the combustion starts at $\sim 235^\circ$ and finishes at $\sim 280^\circ$. Cylinder five was in its combustion phase between $115^\circ - 160^\circ$ and cylinder six between $355^\circ - 400^\circ$. Because there is no overlap it is clear that only one cylinder is in its combustion phase each time instance meaning that the requirement is fulfilled for a 6-cylinder engine. During the

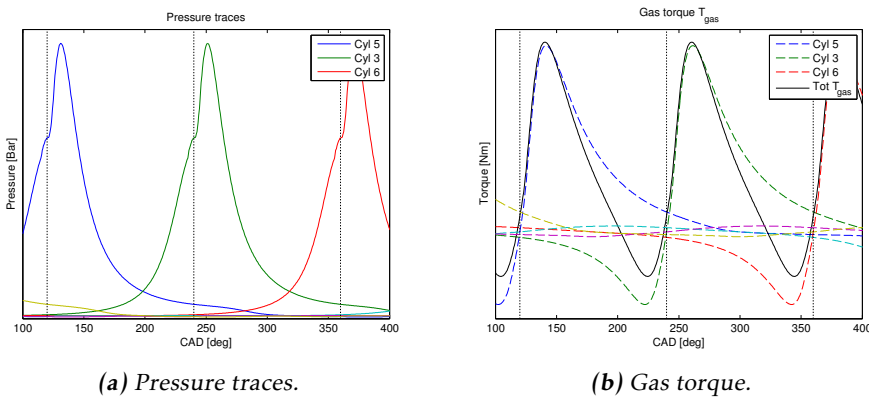


Figure 2.8: Pressure traces for three cylinders and corresponding gas torques. Vertical dashed lines indicate TDC.

interval when cylinder three is firing, adiabatic models for cylinders five and six can be assumed. The rest of the cylinders, which are in the gas exchange cycle, can be assumed to have the same pressure as the intake or exhaust manifold.

In figure 2.8b the gas torque from each cylinder is shown. It is obvious that all cylinders affect the total torque of the crankshaft during the combustion phase of cylinder three thus models of the pressure for the rest of the cylinders is needed. This thesis uses the measured pressure from cylinder six as a first approach to see what kind of results that can be made.

The torque contribution from the non-combusting cylinders can then be removed from the total torque T_{cs} calculated from the CAD-signal after being sent through each SISO system $H_i(j\omega)$.

The remaining torque signal will be the contribution of the cylinder which is in its combustion phase together with crankshaft oscillations due to torsion. To remove the oscillations this signal will be filtered through the inverse SISO system $H^{-1}(j\omega)$ for the cylinder which is in its combustion phase. The output will be all the torque contributions from that cylinder. By subtracting the mass and friction torque from this signal the gas torque is extracted. The cylinder separation is shown in Figure 2.9.

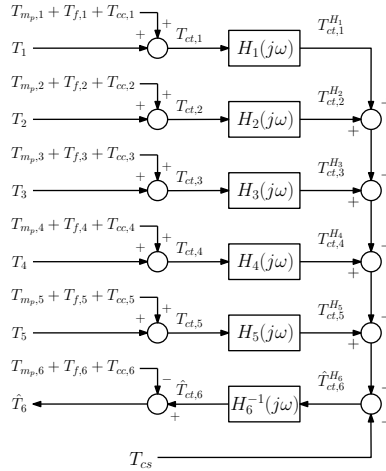


Figure 2.9: Cylinder separation strategy. Here the torque contribution of cylinder six is separated.

With an estimation of the gas torque it is possible to calculate the cylinder pressure by using the inverse crank-slider function or can be estimated by using a Kalman filter estimator.

3

Experimental setup

To be able to design and validate the models, experiments have been performed. This has been done on a Scania DC13 engine in a test cell. The experiments were performed together with other thesis workers and some of the collected data was never used in the development of the VS in this thesis.

The engine specific data is presented in Table 3.1.

Table 3.1: Engine specification.

Engine	DC13
Firing sequence	1-5-3-6-2-4 each 120°
Displaced Engine Volume	12,74 dm ³

3.1 System overview

An overview of the experimental setup can be seen in Figure 3.1. There are two main groups of measured data sets. One group was continuously sampled with a high frequency and the other was averaged data. The continuously sampled signals are CAD based and most are sampled every 0.1 CAD, these measurements are listed below.

- In cylinder pressure. This was measured on the 1st and 6th cylinders.
- Crank angle encoder. The CAD was measured using an optical sensor every 0.5 degrees. These measurements are then interpolated to yield a resolution of 0.1 degrees.
- Intake/Exhaust pressure.

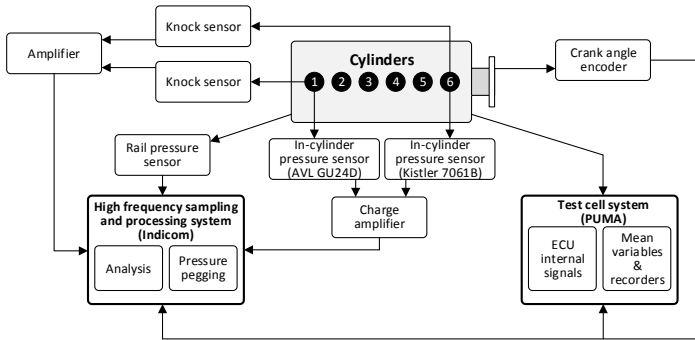


Figure 3.1: An overview of the experiment setup in test cell. (Reproduced with permission from Johansson (2015)).

- Rail pressure. This signal was sampled in the time domain with a frequency of 50 kHz.
- Knock sensors. These sensors were mounted on the exhaust side of the cylinder block. Two sensors were mounted on the engine, one on cylinder one and the other on cylinder six.

This list includes the measurements which are averaged over one or several engine cycles.

- Intake/Exhaust temperatures.
- Brake torque. The produced torque from the engine was measured as an average over an engine cycle. This was measured through the dynamometer.
- NO_x sensor. This sensor measures the oxygen level in the exhaust gases. This is then used to calculate Lambda (air/fuel mixture).
- Oil temperature. Temperatures in the oil were measured on several positions on the engine e.g. oil sump, piston gallery and temperature differences over auxiliary components.

Some signals were model-based and calculated in the ECU. These signals were available and was saved alongside the other data sets. The signals are listed below.

- Estimated amount of fuel injected.
- SOI.
- SOC.
- Fuel amount in the main and pilot injection.

3.2 Experimental procedure

The test were divided into stationary working points, dynamic ramps, adjusted SOI and long term oil degradation tests. In this master's thesis, data from the stationary working points is used to evaluate the virtual pressure sensor and engine simulations.

Stationary working points A total of 36 working points were tested. Each working point consist of an engine speed and an engine load. Each load was tested for each speed. The working points can be seen in figure, 3.2. The experiment

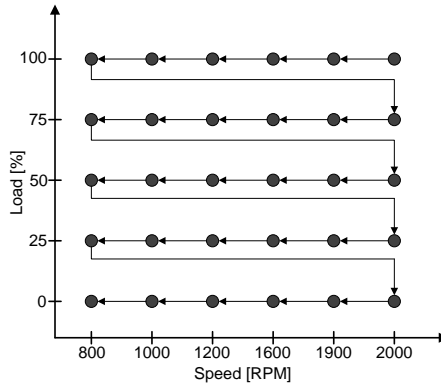


Figure 3.2: Stationary working points. (Reproduced with permission from Johansson (2015)).

was conducted so that one starts in a high load and speed. Then the speed is decremented from the highest to the lowest speed. Then the load case was decremented one step and the speed varied as before. This was repeated until all working points had been tested, see figure 3.2.

For each working point the engine was assumed stabilized when the exhaust gases had reached a steady state temperature. Then the measurements were performed on approximately 50 engine cycles. This process took around 5 min.

Dynamic ramps The ramps were performed in speed and in load. The ramp was performed in a similar manner as before with the exception of a continuously varying load or speed. Each ramp was repeated three times. The test cases were,

- Constant load, ramp in speed. This was made for a constant load of 50%. Two different starting speeds were used, 800 and 1200 RPM. The slope of the ramp was 40 RPM/s over 5 seconds.
- Constant speed, ramp in load. Two test were performed. The first one started with engine speed 1200 RPM and 1200 Nm torque. During the

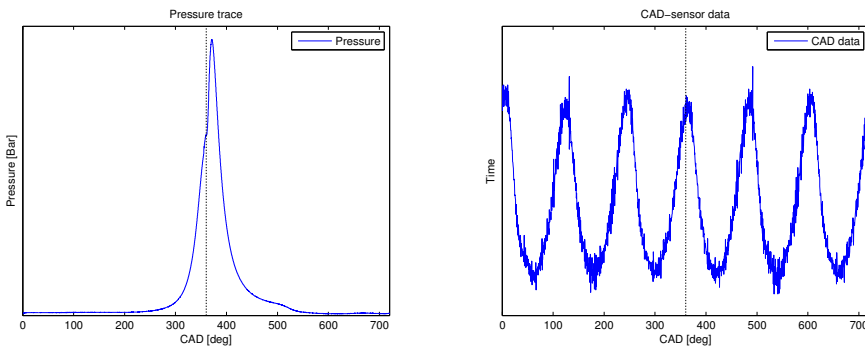
second ramp the initial engine speed was set to 1500 RPM and 800 Nm torque. Each ramp in torque were set to 100 Nm/s over 5 seconds.

Adjusted SOI During these tests the engine load 75% was kept constant. The tests were made for two engine speeds, 1200 RPM and 1900 RPM. For these two cases the fuel injection timing was changed between $0, \pm 2, \pm 10$ CAD.

Oil temperature The engine was kept running during nights to allow for more long term experiments of the oil degradation.

3.2.1 Data collected

In this thesis the CAD-sensor data is of great importance together with measured in-cylinder pressure. In Figure 3.3a a pressure trace from one of the stationary operating points is show. The goal of this thesis is to be able to reconstruct this pressure trace by using the CAD-sensor data signal which is shown in Figure 3.3b. The CAD-sensor data was also used to validate that the engine specific parameters were correct.



(a) Pressure trace from the pressure transducer. (b) CAD data from optical CAD-sensor.

Figure 3.3: Examples of data collected during the experimental procedure. Both data sets are shown for one engine cycle.

4

Torque modeling

In Section 2 models describing the gas and mass torque are given. To be able to simulate the engine from in-cylinder pressure to flywheel acceleration using the torque balancing equation, models of the remaining torques is needed. This section sums up the friction and auxiliary models. This makes it possible to simulate the engine by connecting all torque models with the rigid body or dynamic model of the crankshaft. Also the modeling of the CAD-sensor data to an estimate of the total torque is described.

4.1 Friction models

The friction models available within Scania were estimated on an engine similar to the one used in the experiments for this thesis. The models were derived and validated from engine strip down experiments. The principle of an engine strip down test is to remove components in the engine step by step and perform motored tests at different engine speeds and look at the difference in torque needed. The resulting models are of mean effective pressure type (MEP).

By using the following expression the average torque per cycle can be calculated from the MEP models.

$$T = \frac{MEP \cdot 10^5 \cdot V_D}{2\pi \cdot n_r} \quad (4.1)$$

Here V_D is the volume displaced per cycle and n_r is the number of revolutions of the crankshaft to complete an engine cycle. Since the MEP models are given in Bar the conversion factor is needed to get the pressure expressed in Pascal.

Crank train The friction contributions for the crank train are main bearing, sealing, cam shaft bearing and transmission. The friction model for the crank train is.

$$MEP_{crank} = K_{cr1} + K_{cr2} \cdot n_{eng} + K_{cr3} \cdot n_{eng}^2 \quad (4.2)$$

The crank train friction increases with engine speed.

Piston group The friction contributions in the piston group comes from the ring package, skirt, big and small end bearings. The friction model was derived between motored engine tests with and without pistons and connecting rods. The friction model is expressed as.

$$MEP_{piston} = K_{pi1} + K_{pi2} \cdot n_{eng} + K_{pi3} \cdot n_{eng}^2 \quad (4.3)$$

The friction increases with engine speed.

Valve train The friction contribution for the valve train are cam/roller contact, roller tappet, pushrod, rocker arm, valve bridge pin and the valve guide. See Figure 4.1.

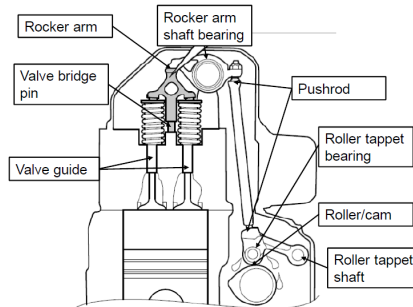


Figure 4.1: Valve train. (Reproduced with permission from Scania).

The MEP model for the valve train is.

$$MEP_{valve} = K_{val1} + K_{val2} \cdot n_{eng} + K_{val3} \cdot n_{eng}^2 \quad (4.4)$$

Oil temperature compensation The friction models above have been calibrated for one oil temperature. Since it is known that the friction is dependent on the oil temperature a compensation model is introduced.

$$MEP_{oil} = K_{oil1} + K_{oil2} \cdot T_{oil} + K_{oil3} \cdot T_{oil}^2 \quad (4.5)$$

With lower oil temperature the friction increases.

Motoring vs firing These models capture the friction torque during motored conditions. During firing condition the contact forces will change on the different components and as a result the friction will change.

For example during the combustion phase the piston will move about inside the cylinder and thus the ring package will exert greater forces on the cylinder liner. Also the bearings friction in the big and small end will increase. Another example is that the pressure difference between the exhaust manifold and cylinder will affect the valve plate differently during the opening of the valve after combustion. This will in turn affect the load on the valve train. Deriving models of the friction during firing condition is very difficult task.

4.1.1 Dynamic crankshaft friction input

When simulating the engine with a dynamic crankshaft model all of the above mentioned friction models will be summed together and included in T_{load} in Eq. (2.25), load at the flywheel.

4.2 Auxiliary models

In Section 2.1.4 the different auxiliary units are listed. In this section the torque models of the different units will be described. Some of the auxiliary units mounted on the test engine was not engaged during the experiments in the test bench.

4.2.1 Drive belt side

Alternator: The alternator is modeled as a static torque contribution. The following model is based on the balance between mechanical and electrical power.

$$T_{alt} = \frac{U \cdot I}{\eta \cdot \omega_{alt}} \quad (4.6)$$

U is the voltage from the alternator and I the current requirement. ω_{alt} is the rotational speed of the alternator and η its efficiency. The torque affecting the crankshaft depends on the gear ratio GR_{alt} between the crankshaft and alternator

$$T_{crank\ alt} = GR_{alt} \cdot T_{alt} \quad (4.7)$$

The alternator was disengaged during the experiments in the test cell, $I = 0$. Still it was connected and driven by the drive belt. Instead of using the model above the torque needed was set to a constant $T_{crank\ alt}$.

AC-compressor The torque needed to drive the AC-compressor depends on if it is engaged or not. Both states are modeled as constant. As for the case of the alternator the AC-compressor was connected with drive belt and disengaged during the experiments.

Coolant pump The coolant pump mounted on the engine in the experiments was of high performance type. Different types of coolant pumps are used depending on engine.

By using data previously collected in a test rig and perform polynomial fitting in least-squares sense the following equation express the relation between needed pump torque and pump speed.

$$\begin{aligned} T_{cool} &= K_{co1} + K_{co2} \cdot n_{pump} + K_{co13} \cdot n_{pump}^2 \\ n_{pump} &= GR_{cool} \cdot n_{eng} \end{aligned} \quad (4.8)$$

The coolant pump has a gear ratio GR_{cool} to the engine speed thus the torque affecting the crankshaft becomes.

$$T_{crank\ cool} = GR_{cool} \cdot T_{cool} \quad (4.9)$$

4.2.2 Transmission side

Oil pump: A model describing how much power the oil pump needs at a given point is as follows.

$$\dot{E}_{oil} = \frac{n_{eng} \cdot GR_{pump} \cdot V_{pump} \cdot \eta_{vol} \cdot (P_{aft} - P_{bef})}{600} \quad (4.10)$$

Here n_{eng} is the engine speed, GR_{pump} is the gear ratio between the crankshaft and oil pump and V_{pump} is the volume size of the pump. The difference in pressure before and after the pump $P_{aft} - P_{bef}$ is a polynomial function calculated from data from engine tests and depends on the pump speed $n_{oil} = GR_{oil} \cdot n_{eng}$ and oil temperature T_{oil} . The volumetric efficiency η_{vol} is modeled from rig measurements. This is modeled as polynomial functions depending on the oil pump speed and pressure difference. The power becomes a function depending on oil temperature and engine speed. The MEP model for the oil pump becomes.

$$MEP_{oil} = \frac{1200 \cdot \dot{E}_{oil}}{n_{engine} \cdot V_{engine}} \quad (4.11)$$

Air compressor: The air compressor can either be loaded or unloaded. The case when the air compressor is loaded it increases the pressure in the storage tank. The compressor mounted on the engine have two pistons where each piston compresses air once during a revolution of the axis they are connected to. Due to this the torque needed oscillates twice during an axis revolution. The torque also depends on the pressure in the storage tank and the speed of the engine. Unfortunately no model that capture the dynamics of the air compressor at the loaded case exist at the moment.

The following MEP model was build from rig measurements of an unloaded air

compressor.

$$\begin{aligned}MEP_{air} &= K_{air1} + K_{air2} \cdot n_{air} + K_{air3} \cdot n_{air}^2 \\ n_{air} &= GR_{air} \cdot n_{eng}\end{aligned}\quad (4.12)$$

The air compressor was never loaded during experiments in the test cell so the MEP model was used.

Even with an accurate torque model of the loaded case, the gear ratio with the crankshaft makes it difficult to phase the oscillating torque curve with the crankshaft.

Fuel pump: Since the high pressure part of the fuel pump is of piston type the torque needed to drive it oscillates during a revolution. The fuel pump mounted has got two pistons, each piston pumps fuel to the common rail two times during one revolution of the shaft which is of cam type. The fuel pump has a gear ratio of one relative the crankshaft and thus four pulses occur during a revolution of the crankshaft. Since it has gear ratio one relative the crankshaft the pulses occur at the same CAD cycle after cycle. Simulated data with the torque oscillations in the form of a look-up table from CAD to fuel pump torque was found. A problem is that when the fuel pump is installed on the engine it is not phased in an exact way to the crankshaft, which e.g. the camshaft is. Because of the fluctuation it is important that the simulated data is phased correctly to be of any use. Instead a static mean value model in the form of look-up tables has been used.

Camshaft: The torque needed for the camshaft to open the intake and exhaust valves depends on the operating point. The valves are only open during the gas exchange strokes and because of a overlap with intake and exhaust valves the camshaft consumes energy during this interval. When the valves are open the springs will store energy which will be returned when the valves are closed and thus the camshaft returns some torque. From simulated data the torque oscillates six times during one revolution of the camshaft because of six gas exchange strokes.

Hydraulics pump: During the experiments in the test cell the hydraulics pump needs considerably less torque compared to when the engine is mounted in a truck. In the test cell the pump is only dragged. Thus a constant torque value T_{hyd} is set.

4.2.3 Fan

Fan model: The model that describes the amount of torque the fan needs at a given engine speed is as follows.

$$T_{fan} = K_{fan1} + K_{fan2} \cdot n_{eng} + K_{fan3} \cdot n_{eng}^2 \quad (4.13)$$

The model above is fitted to data when the viscous clutch is fully engaged, which was the case when experiments are conducted in a test cell.

4.2.4 Dynamic crankshaft auxiliary inputs

When simulating the engine with a dynamic crankshaft model the auxiliary models will be split up in two groups. All auxiliary systems on the drive belt side will, together with the fan, become a summed torque input to node two $T_{aux,2}$ in Eq. (2.23). The auxiliary systems connected to the transmission side will be a summed torque input $T_{aux,9}$ to node nine, together with the friction and load torque Eq. (2.25).

4.3 Estimated torque from CAD-data

This section describes the signal processing of the CAD-sensor data. The optical sensor register when a hole on the marker disk passes by. At the same time a fast clock times the elapsed time from previous hole, T_i . Since the marker disk has a resolution of 0.5° , each engine revolution will get 720 time samples. To calculate the instantaneous engine speed the following equation is used.

$$\dot{\theta}_i = 2\pi \cdot \frac{1}{720 \cdot T_i} \quad (4.14)$$

4.3.1 Filtering the CAD-signal

The engine speed is synchronous with CAD. This signal is re-sampled with an equidistant time by using Matlabs `interp1` function. The equidistant sampling time is set to $t_s = t_{360^\circ}/720$ where t_{360° is the total time of one revolution of the crankshaft. Without the interpolation the frequency content of the signal will be misinterpreted when analyzing it with the FFT and also the filtered signal will be different when sent through a low-pass filter. The resulting $\dot{\theta}$ is shown in Figure 4.2. Also shown is the result when $\dot{\theta}$ is differentiated by using the central difference rule to avoid phase shift. The resulting $\ddot{\theta}$ is very noisy and it is evident that the engine speed signal needs to be filtered before being differentiated.

The frequency content in the CAD-signal changes with engine speed. Thus the filter cut-off frequency needs to be adjusted depending on engine speed. When analyzing the frequency content of a rotating system with overloaded frequencies it is normal to talk about oscillations per axle revolution. The frequencies will then be normalized with the engine speed. One oscillation per axle revolution will be referred to engine order one. Instead of setting a cut-off frequency in [Hz] in the filter, the cut-off is designed with respect to engine order. In this thesis work, data from stationary operating points was used and a low-pass filter was designed for each engine speed. Since the data was processed off-line a non-causal filter was used. A fifth order low-pass Butterworth filter was used together with Matlab function `filtfilt` to perform the filtering. The decision of using a fifth order Butterworth filter was made by analysing the FFT after the CAD-signal was filtered.

In order to decide at which engine order the cut-off should be set, different cut-offs were tested. In Figure 4.3 the results of six different cut-offs are shown when

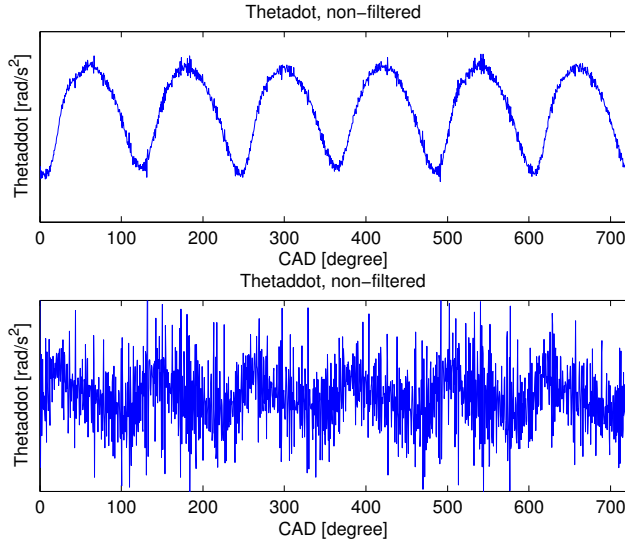


Figure 4.2: Non-filtered engine speed signal above. The differentiated signal below.

applied to angular speed $\dot{\theta}$ which was then differentiated to get the angular acceleration $\ddot{\theta}$.

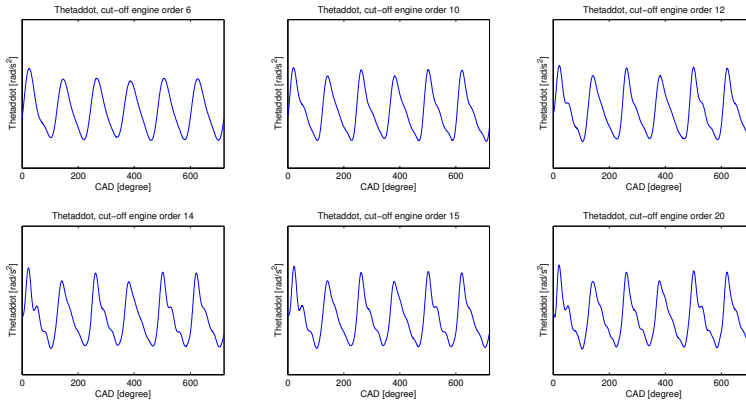


Figure 4.3: Modeled $\ddot{\theta}$ from CAD-signal filtered with different cut-off frequencies, engine orders.

The decision where to set the cut-off order was a difficult task. It was based on the engine simulations described in the next section. When compared with the rigid body crankshaft model the cut-off was set too low and removed torsional effects

from the signal. This was evident later in the thesis work when the dynamic crankshaft model was simulated. In the end the cut-off was set to the 15th engine order.

In Figure 4.3 the oscillating behavior on the retardation is due to crankshaft torsion. Also the shape of the peaks are due to torsion. Even at low engine speeds, as shown in figure, this phenomenon exist in a heavy duty engine.

4.3.2 Torque estimation from CAD-signal

With the angular acceleration $\ddot{\theta}$ of the crankshaft known a torque estimation can be calculated by multiplying it with the crankshaft inertia. Since the inertia is depending on crankshaft angle $J(\theta)$, it is crucial to phase it correctly. The resulting torque model from CAD-data becomes

$$T_{CAD}(\theta) = J(\theta) \cdot \ddot{\theta}. \quad (4.15)$$

4.4 Engine simulations

With the friction and auxiliary models stated in previous sections, the complete engine can now be simulated. All engine specific parameters have been collected from data sheets over the different components.

4.4.1 Rigid body crankshaft

First, the engine is simulated with a crankshaft that is assumed to be a rigid body. The sum of all torques affecting the crankshaft is the right hand side of Eq. (2.16).

$$T_{rbm}(\theta, \dot{\theta}) = T_{gas}(\theta) - f(\theta)\dot{\theta}^2 - T_{fric}(\theta) - T_{load}(\theta) - T_{aux} \quad (4.16)$$

This rigid body model results in a torque trace that is periodic with 120° because the torque models are constant or periodic with 120° . In Figure 4.4 three different engine speeds at 50% load are simulated. Because of the periodic signal, it is interesting to analyze T_{rbm} between two combustions, e.g. 0° to 120° , to see how the different torque models affect the total rigid model output.

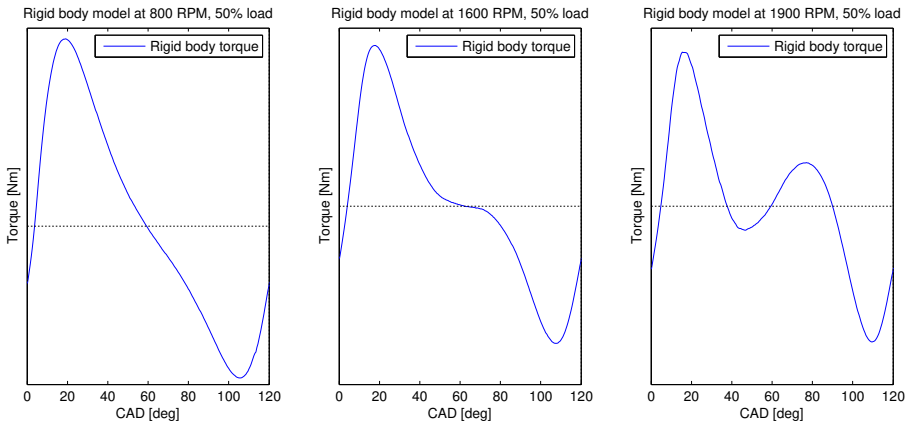
The torque measured in the test bench T_{load} , which is constant for an operating point, has been subtracted for all CAD. At 0° the torque is negative. This is mainly because of the load. Friction in the engine and the torque needed to drive the auxiliaries contribute to negative torque. Also the cylinder next to go into the combustion phase is starting its compression phase. Still the cylinder that is in its expansion phase gives a positive torque contribution. The cylinder which currently is in its combustion phase is at TDC and does not give any torque contribution since the lever in the crank-slider mechanism is zero. Figure 2.8b shows that the gas torque from the three mentioned cylinders mainly affect the crankshaft in a 120° region.

Between 5° - 60° the torque from the firing cylinder dominates and the magnitude is proportional to the in-cylinder pressure. In the same interval energy gets

stored in the moving masses within the engine. Still torque is needed for friction, auxiliaries and the compressing cylinder.

After 60° the shape of T_{rbm} looks different depending on the engine speed $\dot{\theta}$. Since the mass torque depends on $\dot{\theta}^2$, with increasing speed more energy is stored in the masses. In a heavy duty engine the pistons and connecting rods have considerably larger mass in comparison to a car engine.

The stored kinetic energy in the masses are returned between 60-120 degrees. The mass torque phenomenon is seen with increasing engine speed. This is clearly showed in Figure 4.4. At 1600 RPM the return of energy, mass torque, is clearly seen and it is even more evident at 1900 RPM when a local torque maximum occurs. The cylinder that undergoes compression is the main factor to the negative torque at this interval and has got a local minimum at $\sim 100^\circ$. After this point the torque needed to continue the compression becomes less due to that the lever arm decreases as the piston is moving towards TDC. By studying the interval $0^\circ - 120^\circ$ in Figure 4.4 the main difference in shape is due to the mass torque.



(a) 800 RPM at 50% load (b) 1600 RPM at 50% load (c) 1900 RPM at 50% load

Figure 4.4: Simulation results from different engine speeds when the rigid body crankshaft model is used.

4.4.2 Dynamic crankshaft

By introducing a nine degree of freedom lumped torsional vibration model, see Figure 2.6, the crankshaft gets a dynamic behavior. With all torque models set correctly to each mass, the simulation will calculate the angular speed $\dot{\theta}_{dcm}$ of the flywheel. The estimated torque output from this model is calculated in a similar way as the estimation of torque from the CAD-sensor. First the output is filtered with the non-causal filter with the cut-off designed for the engine speed, then it is

differentiated in the same way as described in Section 4.3.1. Then the crankshaft inertia $J(\theta)$ is phased correctly to $\ddot{\theta}_{dcm}$. The estimated torque from the dynamic crankshaft model becomes

$$T_{dcm}(\theta) = J(\theta) \cdot \ddot{\theta}_{dcm}. \quad (4.17)$$

In Figure 4.5 a torque trace for an engine cycle is shown. The static operating point simulated is 1200 RPM and 50% load. The torque trace is no longer periodic with 120° , as it was with a rigid body crankshaft model. Instead it is periodic with 720° . The shape between two vertical TDC lines, 120° , depends on how far away the firing cylinder is from the flywheel. The first peak after TDC is narrower and the magnitude is greater the further away the firing cylinder is. Also the second peak is more distinguished in that case. This indicates that the torsion is greater in the crank lever further down the crankshaft relative to the flywheel. With a spring-mass-damper model of the crankshaft the oscillating behavior in the torque trace increases with engine speed. Still at the operating points run at the lowest engine speed, 800 RPM, oscillations occur that was not captured with the rigid body model.

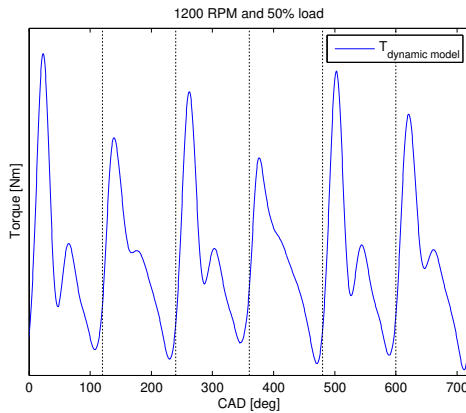


Figure 4.5: Modeled torque with a dynamic crankshaft model. The vertical lines indicate when the firing cylinder is at TDC.

5

Results and discussion

In this section comparisons between the estimated torque calculated from the CAD-sensor data T_{CAD} and engine simulations are done. The first comparison is between calculated torque on the flywheel T_{rbm} using the rigid body crankshaft model and T_{CAD} . Then T_{CAD} is compared with the flywheel torque T_{dcm} from engine simulations using the spring-mass-damper model of the crankshaft to model the torsional effects. In order to estimate the torque contribution of a single cylinder, the cylinder separation was done with a rigid body model. The estimated torque trace from the separation is then used to estimate the in-cylinder pressure.

5.1 Comparison between T_{CAD} and T_{rbm}

The rigid body crankshaft torque model is compared with the torque model estimated from the CAD-sensor data. The two models will be compared over a complete engine cycle for different operating points.

Here the simulated torque trace from the rigid body model is the summed torque contributions from the different torque models described in previous chapters.

$$T_{rbm}(\dot{\theta}, \theta) = T_{gas} - f(\theta)\dot{\theta}^2 - T_{aux} - T_{fric} - T_{load} \quad (5.1)$$

The measured CAD-signal has been modeled to get an estimate of the flywheel torque according to Section 4.3.

$$T_{CAD}(\theta) = J(\theta) \cdot \ddot{\theta} \quad (5.2)$$

The two equations above are the right and left hand side of the torque balancing equation, Eq. (2.5). If T_{rbm} captures all phenomenon between the pressure inside

the cylinders to the flywheel the two torque traces should be equal and overlap each other. The results are shown in Figure 5.1. In addition to the two signals the difference $T_{error} = T_{CAD} - T_{rbm}$ between them is also shown.

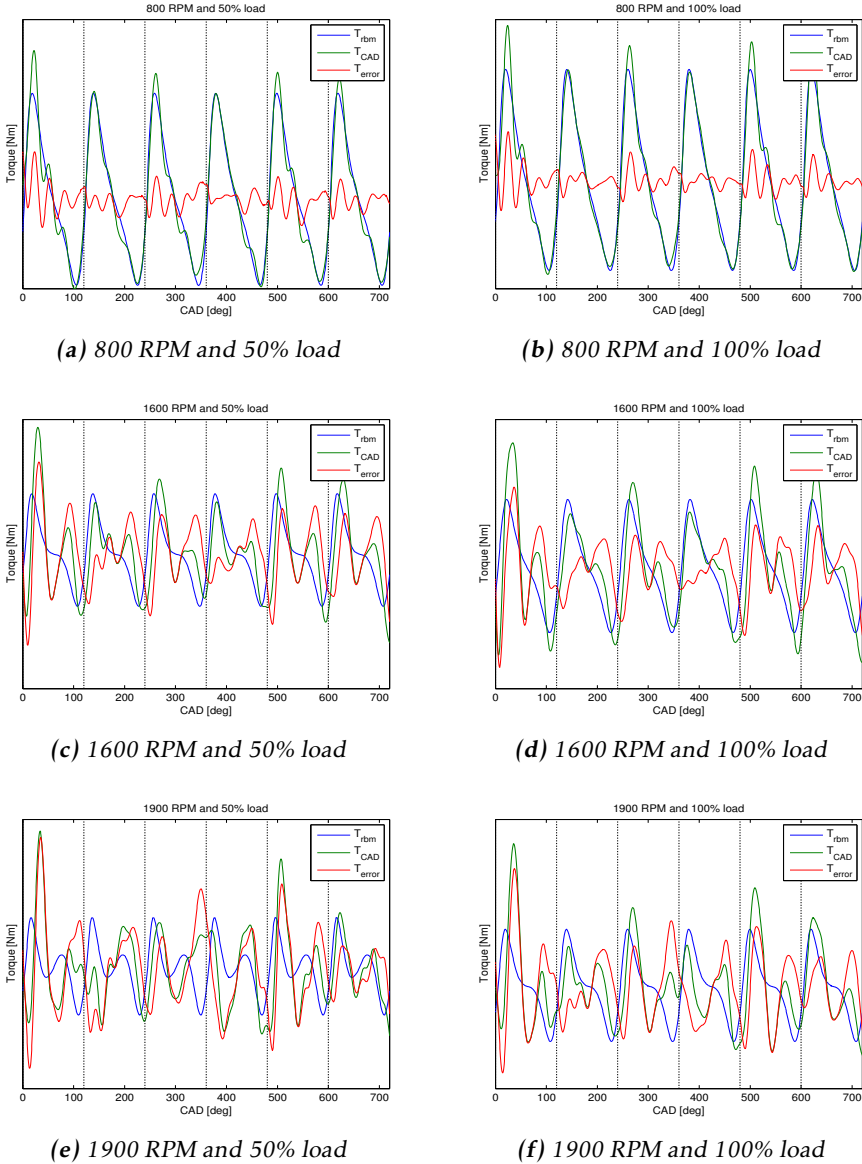


Figure 5.1: Comparisons between T_{CAD} and T_{rbm} at six different operating points. The vertical dotted lines indicates when the firing cylinder is at its TDC.

5.1.1 Discussion

The rigid body model is compared with the estimated torque derived from the CAD-signal for three different engine speeds 800 RPM, 1600 RPM and 1900 RPM. Two load points are tested for every engine speed, 50% and 100 % load. The firing sequence in a six cylinder inline engine is 1, 5, 3, 6, 2, 4. The engine simulations with a rigid body crankshaft model uses the measured in-cylinder pressure from cylinder six as input to all cylinders, thus making the total gas torque periodic with 120° . In the real case each cylinder pressure deviates slightly. Due to the shape of the inlet manifold each cylinder can not get the same amount of air during the intake stroke. The engine temperature is not constant for all cylinders, the front end of the engine is cooler due to better air flow. It is also less heated by the rest of the cylinders. The fuel injectors might differ in the amount of fuel injected. Since not all the cylinders were fitted with pressure sensors in the test bench, pressure data from cylinder six was used.

In Figures 5.1a-b the comparison between the two torque models at 800 RPM for 50% and 100 % load is shown. The modeled torques overlap quite well at this engine speed. Still there are some parts of the T_{CAD} trace that is not captured by T_{rbm} . Most notable in T_{CAD} is that the maximum torque peak is different depending on which cylinder that is firing (Discussed below). Also after the maximum peak there is a oscillating behavior when the torque is decreasing. One also notice that when the firing cylinder is further away from the flywheel the estimated torque maximum in T_{CAD} is more delayed. The greater the maximum peak, a more oscillating behavior is observed. This can be seen clearly in the figures. The torque difference T_{error} clearly shows that it is not only during the two mentioned sections that there is a difference between the two models. Even when it looks like they overlap well there is a difference. The error is smallest between 360° - 480° when cylinder six is firing.

The maximum torque peak and oscillating behavior can not be explained by lack of pressure data for all cylinders, since the pressure difference between cylinders is not that large. The origin of this error can nor be explained by faulty friction or auxiliary models since the magnitude of the error is much larger. Also the period does not coincide with any of the auxiliaries with changing torque depending on the CAD, camshaft and fuel pump.

Table 5.1: Mean absolute torque error between rigid body model and CAD torque for each cylinder at 800 RPM. The mean error is calculated from TDC to 120° after TDC.

	Cyl 1	Cyl 2	Cyl 3	Cyl 4	Cyl 5	Cyl 6
50%	250 Nm	200 Nm	200 Nm	150 Nm	150 Nm	100 Nm
100%	450 Nm	300 Nm	300 Nm	250 Nm	200 Nm	150 Nm

In Table 5.1 the mean absolute error for each 120° region for both load cases at 800 RPM is shown. The largest error is found in the angle area when cylinder one is firing. One must remember that cylinder one is in the front end of the engine

and furthest away from the flywheel. More likely to explain the oscillating torque error is that the crankshaft is easier to twist from cylinder one. The torsional effects stores energy in the crankshaft when it gets turned up. Later this energy will be returned when the crankshaft untwist itself. This is probably the reason for the oscillatory behavior seen in the torque error between T_{CAD} and T_{rbm} . In Table 5.1 the trend is that the error decreases when the firing cylinder is closer to the flywheel. The reason why the error is not declining "cylinder by cylinder" in the table could be because each 120° region is not only affected by the firing cylinder. But the error for cylinder one is always larger in mean compared to cylinder six.

The increase of T_{error} at the higher load is explained by that more energy is released in the engine. This leads to larger torsion since the energy has to pass via the crankshaft to the flywheel.

In Figure 5.1c-d comparisons between the two torque models at 1600 RPM for 50% and 100 % load is shown. The torsional effects are more evident when the engine is running at 1600 RPM. This is probably due to that the frequency of the induced oscillations, combustion and mass torque, are closer to the natural frequency of the crankshaft. At 800 RPM the oscillations were superimposed during the decrease in T_{CAD} . At 1600 RPM T_{CAD} oscillates wildly in the decrease torque regions and are not as smooth as T_{rbm} . This is a phenomenon that the rigid crankshaft model is unable to capture resulting in a big difference between T_{gas} and T_{rbm} . The error even has the same magnitude as T_{rbm} meaning that a rigid body crankshaft model is not suited to be used at this engine speed.

Table 5.2: Mean absolute torque error between rigid body model and CAD torque for each cylinder at 1600 RPM. The mean error is calculated from TDC to 120° after TDC.

	Cyl 1	Cyl 2	Cyl 3	Cyl 4	Cyl 5	Cyl 6
50%	1800 Nm	1250 Nm	1100 Nm	1100 Nm	800 Nm	650 Nm
100%	2550 Nm	1800 Nm	1350 Nm	1350 Nm	1100 Nm	900 Nm

In Table 5.2 the mean absolute error for each 120° region for both load cases at 1600 RPM is shown. The same trend with decreasing error when the firing cylinder is closer to the flywheel also appears here. Overall the same behavior as described for T_{CAD} at 800 RPM can be seen at 1600 RPM. Depending on firing cylinder, torque maximum amplitudes are different and the delays vary. Also there are oscillations during and after the combustion process. The fundamental difference at 1600 RPM is that the engine simulations with a rigid body crankshaft T_{rbm} is far from describing T_{CAD} because the rigid body model is not capable of modeling torsional effects.

Lastly Figure 5.1e-f describes when the engine is running at 1900 RPM. The T_{CAD} signal is very different from the rigid body simulation and it is difficult to see any resemblance between the two. Once again the natural frequency of the crankshaft affects the CAD-signal.

Table 5.3: Mean absolute torque error between rigid body model and CAD torque for each cylinder at 1900 RPM. The mean error is calculated from TDC to 120° after TDC.

	Cyl 1	Cyl 2	Cyl 3	Cyl 4	Cyl 5	Cyl 6
50%	1800 Nm	1350 Nm	1050 Nm	450 Nm	1000 Nm	1000 Nm
100%	2650 Nm	2050 Nm	1900 Nm	1100 Nm	1150 Nm	1550 Nm

In Table 5.3 the trend with decreasing error when the firing cylinder is closer to the flywheel is not as clear at 1900 RPM. Still the error of cylinder one and two is larger than cylinder five and six.

In Table 5.4 the main frequency of the oscillation in the torque error is shown. The period between two tops or bottoms are not always the same, thus the mean period time is used to calculate the frequency.

Table 5.4: Frequency of the oscillations in torque error.

	800 RPM	1600 RPM	1900 RPM
100% Load	160 Hz	190 Hz	190 Hz
50% Load	160 Hz	180 Hz	180 Hz

The first resonant frequency of the crankshaft is around 200 Hz. Why the frequency of the oscillations differs from 200 Hz is unknown.

One reason could be because of the damping wheel mounted on the crankshaft. The damping wheel is fitted in the front end of the engine to minimize the oscillations in the crankshaft so a resonance disaster does not occur. Without a damping wheel the mechanical stress on the crankshaft would exceed the maximum load tolerance and eventually break. It is probable that the damping wheel cancels out oscillations with higher frequencies especially if those oscillations have low amplitudes.

With the assumption that the crankshaft is a rigid body the difference, or error, between the two models are large for all operating points illustrated here. Even at 800 RPM and 50% load where the resemblance between modeled and measured torque is quite good, the maximum instantaneous error is 1 kNm.

5.1.2 Conclusion rigid body

From the section above it is evident that the T_{rbm} and T_{CAD} overlap better at lower RPMs. But still there is a large error between the two models. With increasing engine speed the oscillating mass and gas torques have got frequency content that is close to the natural frequency of the crankshaft resulting in larger torsional effects. The resulting torque error is greater when a firing cylinder is further away from the flywheel. Because the error is so large in magnitude it is impossible to draw any conclusions of the friction and auxiliary models other than that they

are not the cause of it. To minimize the error a dynamic model of the crankshaft must be implemented.

5.2 Comparison between T_{CAD} and T_{dcm}

This section compares the dynamic crankshaft torque model T_{dcm} with the torque estimated from the CAD-sensor data T_{CAD} . A nine degree of freedom spring-mass-damper model simulates the dynamic torsional effects of the crankshaft. The same operating points used when comparing T_{rbm} and T_{CAD} is evaluated here. The results are shown in Figure 5.2 over a complete engine cycle.

5.2.1 Discussion

In Figure 5.2a-b the two torque models at 800 RPM for 50% and 100% load is shown. With the introduction of a dynamic crankshaft model the simulated torque trace captures the phenomenon of different torque maximums after the cylinder is firing. The peaks coincides in the same way as for the T_{CAD} trace. Another improvement is that T_{dcs} captures the first oscillation in the section where the torque is decreasing. The qualitative shape has improved in that sense. By introducing a dynamic crankshaft model the torque trace is no longer periodic with 120° . Still T_{error} reveals that there is a difference between the two models. Even though the different torque maximums are captured in T_{dcm} , there is still a difference in magnitude compared with T_{CAD} . Also T_{dcm} only captures one oscillation in the decreasing torque region where T_{CAD} has got two.

Table 5.5: Mean absolute torque error between dynamic crankshaft model and CAD torque at 800 RPM and the two load cases. The mean error is calculated from TDC to 120° after TDC for each cylinder.

	Cyl 1	Cyl 2	Cyl 3	Cyl 4	Cyl 5	Cyl 6
50%	250 Nm	200 Nm	150 Nm	150 Nm	150 Nm	200 Nm
100%	400 Nm	350 Nm	300 Nm	350 Nm	300 Nm	300 Nm

In Table 5.5 the mean absolute error has the same size as the error when using a rigid body crankshaft, Table 5.1. The introduction of a dynamic crankshaft has resulted in no improvement in quantitative error for the 800 RPM case.

In Figure 5.2c-d the two torque models are shown when the engine is running at 1600 RPM with 50% and 100% load. In comparison with the simulation with a rigid body crankshaft the introduction of the dynamic model has resulted in a completely different torque trace at 1600 RPM. Qualitatively the trace is more consistent with T_{CAD} . The improvement is clearly shown when looking at the instantaneous difference between the two models.

In Table 5.6 the mean absolute error is shown for each 120° for the two load cases at 1600 RPM. The error has decreased in all intervals when compared to Table 5.2 where the errors are shown for the rigid body crankshaft. In the region

Table 5.6: Mean absolute torque error between dynamic crankshaft model and CAD torque for each cylinder at 1600 RPM. The mean error is calculated from TDC to 120° after TDC.

	Cyl 1	Cyl 2	Cyl 3	Cyl 4	Cyl 5	Cyl 6
50%	850 Nm	900 Nm	800 Nm	550 Nm	750 Nm	550 Nm
100%	1150 Nm	1250 Nm	950 Nm	600 Nm	850 Nm	550 Nm

when cylinder one is firing the error has reduced to half. The introduction of a dynamic crankshaft model is one step towards minimizing the error, but the large error still occurring most not be ignored.

The two load cases when the engine is running at 1900 RPM are shown in Figures 5.2e-f. At 50% load T_{dcm} struggles to capture the quick oscillations included in T_{CAD} . In the case when the engine is running at 100% load the simulated torque trace looks somewhat better when comparing with T_{CAD} .

Table 5.7: Mean absolute torque error between dynamic crankshaft model and CAD torque for each cylinder at 1900 RPM. The mean error is calculated from TDC to 120° after TDC.

	Cyl 1	Cyl 2	Cyl 3	Cyl 4	Cyl 5	Cyl 6
50%	800 Nm	700 Nm	900 Nm	750 Nm	1000 Nm	550 Nm
100%	900 Nm	850 Nm	1050 Nm	700 Nm	850 Nm	900 Nm

In table 5.7 there is a small difference in magnitude between the two loads for each region. Even though much more energy goes through the crankshaft at 100% load the error is not much larger. This shows that the dynamic crankshaft model better captures the torsional behavior at 100% load. A comparison with Table 5.3 shows that T_{error} is reduced by introducing a dynamic crankshaft model.

5.2.2 Conclusion dynamic crankshaft

It is evident from Figure 5.2 that the shape of T_{CAD} is highly affected by the torsional effects. The shapes of the two models are more equal now in comparison with the results from the rigid body approach. The spring-mass-damper system captures the torsion phenomenon, but not exactly. One reason could be because the spring, damper and inertia parameters are not correct. Another is that the damping wheel model is simplified. Here the spring and damper parameters are set constant, but in the real case these are frequency dependent. By introducing this frequency dependence the results could become better.

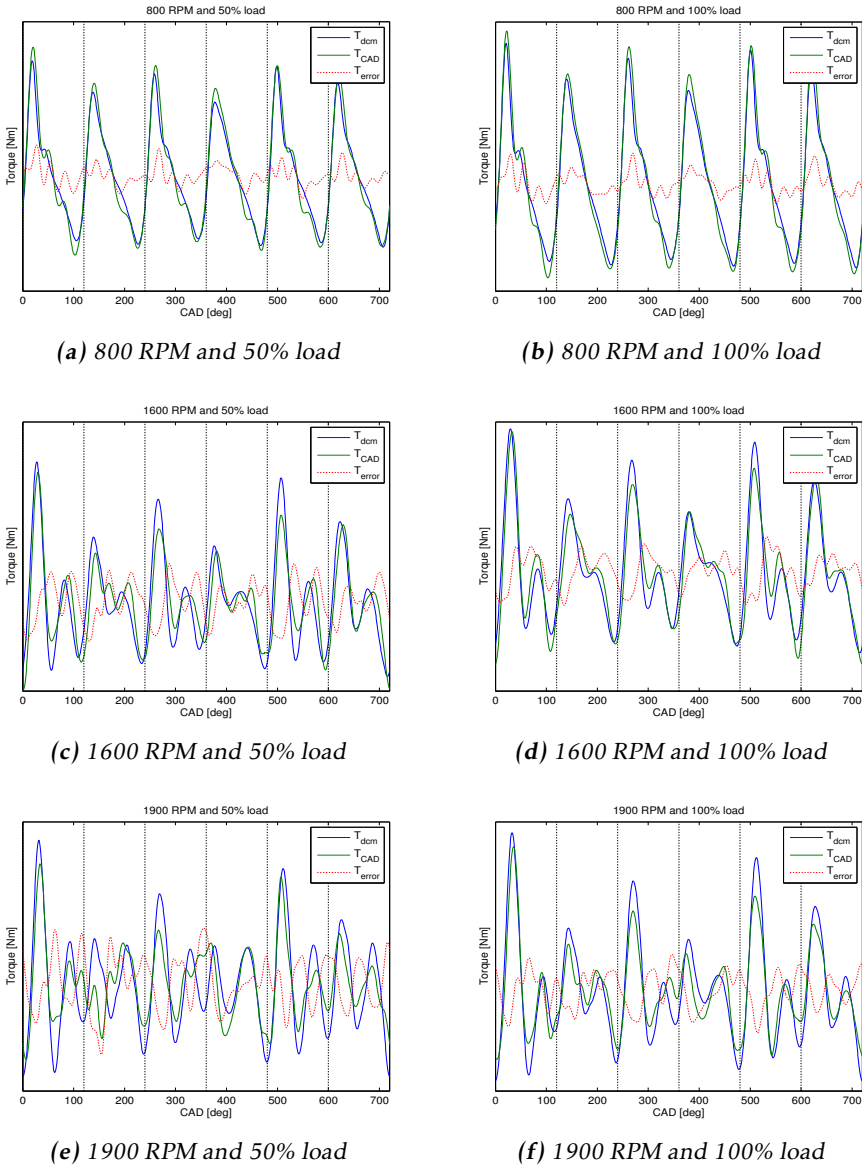


Figure 5.2: Comparisons between T_{CAD} and T_{dcm} at six different operating points. The vertical dotted lines indicates when the firing cylinder is at its TDC.

5.3 Cylinder separation using rigid body model

One goal of this thesis was to use the cylinder separation approach for a dynamic crankshaft described in Section 2.5. Unfortunately, the inverse $H_i^{-1}(j\omega)$ resulted in an unstable system and no results came out of it.

Instead the separation was done with the rigid body crankshaft model. The transfer functions in Figure 2.9 is set to 1. Previous comparisons between T_{CAD} and T_{rbm} in Section 5.1 showed that when cylinder six was in its combustion phase resulted in least torsional effects. That is why the estimation of the gas torque of cylinder six is evaluated. In Eq. (5.1) the gas torque contribution from cylinder six was removed. The gas torque from the remaining five cylinders is summed in T_{gas-6} . The gas torque of cylinder six $\hat{T}_{gas,6}$ is estimated by removing $T_{rbm}(\theta, \dot{\theta})$ with cylinder six turned off from $T_{CAD}(\theta)$

$$\hat{T}_{gas,6} = J(\theta)\ddot{\theta}_{CAD} - T_{gas-6} + T_{mass} + T_{fric} + T_{aux} + T_{load} \quad (5.3)$$

In Figure 5.3 torque traces when the engine is running at 800 RPM are shown. The blue curve is $T_{rbm}(\theta, \dot{\theta})$ without the gas torque of cylinder six. Due to no contribution of torque from cylinder six, T_{rbm} is no longer periodic with 120° . The increase of torque maximum when cylinder three is in its combustion phase is due to lack of compression torque from cylinder six and the decrease in torque maximum for cylinder four is because of no torque contribution from the expansion phase of cylinder six. Also seen in the figure is the modeled torque from the CAD-sensor data T_{CAD} plotted in green. The difference between these two signals, the estimated gas torque of cylinder six $\hat{T}_{gas,6}$ is plotted as red. If both models would capture all dynamics, the estimated torque would be equal to the real gas torque trace from cylinder six $T_{gas,6}$, which is also plotted in the figure in light blue.

The two gas torque traces are showed together separately in Figure 5.4. It can be seen that the estimated gas torque has a very oscillating behavior compared with $T_{gas,6}$ due to torsional effects. The oscillation has the same frequency as shown in Chapter 5. The two torque curves overlap quite well, especially in the region 360° - 410° . The estimated maximum torque is very close to the maximum torque calculated from in-cylinder pressure.

The same procedure as described above was used on data from 1600 RPM and results is shown in Figure 5.5. When the engine is running at 1600 RPM the torsional effect is more evident. This can clearly be seen in the figure when both modeled signals differs from each other and thus the difference between the signals gets larger. In comparison with Figure 5.3 the estimated gas torque signal, red, at 1600 RPM does not follow as closely the torque curve, light blue. The author's judgment is that the curves match qualitatively and that the estimated max torque deviates slightly in comparison with the maximum torque calculated from measured in-cylinder pressure.

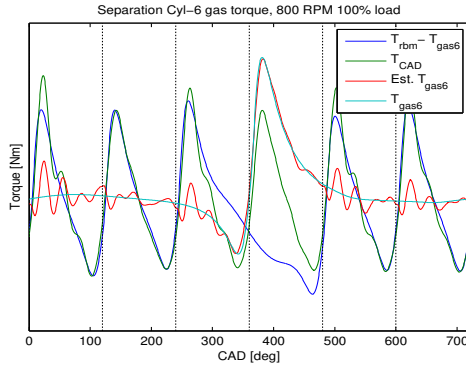


Figure 5.3: Cylinder separation.

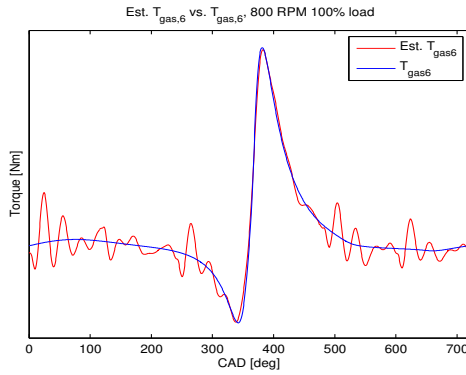


Figure 5.4: Estimated $\hat{T}_{gas,6}$ from cylinder separation versus $T_{gas,6}$ calculated from measured in-cylinder pressure.

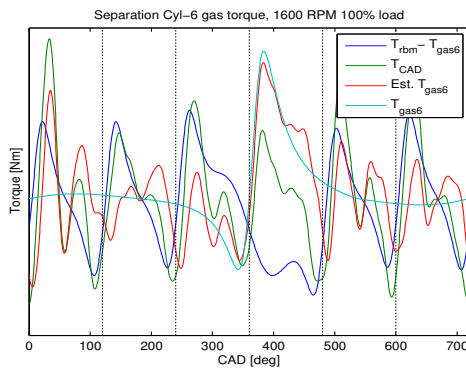


Figure 5.5: Using modeled torque from pressure and CAD to perform cylinder separation. The red and light blue lines should be equal if everything has been modeled.

5.4 Pressure estimation

5.4.1 Inverse crank slider

From the estimated torque from cylinder six in Fig 5.4, the cylinder pressure is reconstructed by using the inverse crank slider function. The resulting pressure curve is plotted in Figure 5.6 together with the measured in-cylinder pressure from cylinder six. As expected the estimated pressure goes to infinity at TDC 360° and BDC at 180° and 480° when division by zero occurs. The reason why the estimated pressure goes towards negative infinity before TDC is because the estimated torque changed sign and became positive before TDC at 360° . The correct gas torque trace is always negative in the region between 180° and 360° , zero at 360° and positive between 360° and 540° .

The estimated pressure has interesting areas at the compression and expansion part of the cycle. The compression is somewhat captured between 310° - 340° and the expansion between 370° - 490° .

A problem with this approach is that there is no pressure estimation around TDC, see Figure 5.7.

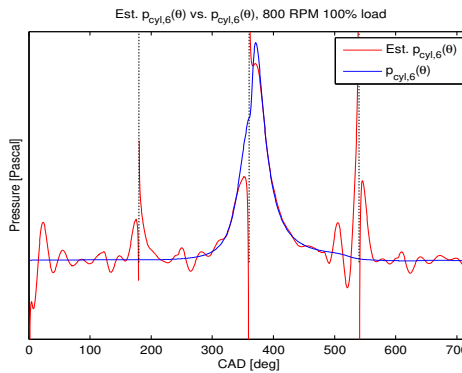


Figure 5.6: Estimated pressure using rigid model and CAD-sensor data at 800RPM and 100% load.

This leads to even larger errors when the inverse crank slider function is used to get in-cylinder pressure at higher engine speeds. The resulting pressure trace at 1600 RPM is shown in Figure 5.8.

It is evident that the estimated cylinder pressure at 1600 RPM is worse than at 800 RPM since the measured and calculated curves only have some resemblance.

By looking at the area 0-300 CAD on the estimated pressure curve in Figure 5.8 it can be seen that the signal is even more perturbed at this engine speed because of the torsional effects due to previous combustion. Also the expansion phase has got a big bump at $\sim 450^\circ$ which is due to torsional effects from cylinder six firing. Some parts of the compression and expansion is still captured at 1600 RPM.

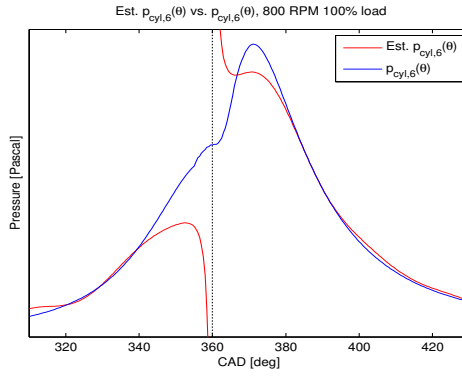


Figure 5.7: Zoomed pressure traces from Figure 5.6.

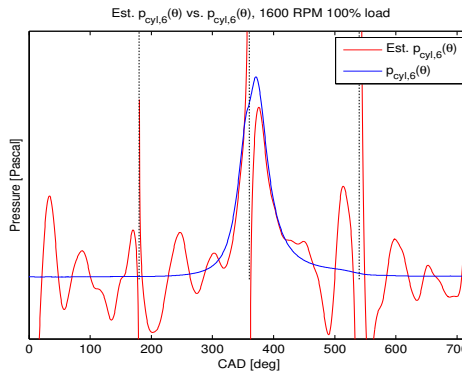


Figure 5.8: Estimated cylinder pressure versus measured at 1600 RPM and 100% load.

5.5 Kalman filter pressure estimation

To avoid division with zero a Kalman filter approach was used to estimate the pressure. The results from the Kalman filter pressure estimator is shown in figures 5.9-5.11 together with measured in-cylinder pressure of cylinder six. The pressure estimation is better at lower engine speeds in the same way and for the same reasons as in Section 5.4.1.

In Figure 5.9 the engine is running at 800 RPM at 50% and 100% load. Both estimated pressures has some oscillating behavior between 0° - 300° and between 430° - 720° in comparison with the measured pressure. The reason is that the rigid body model is unable to capture the torsional effects. Between 300° and 355° the compression is somewhat captured until some degrees before TDC. The Kalman filter circumvents the division by zero so the estimated pressure does not go to infinity close to TDC. Still the Kalman pressure estimator has difficulty to follow the measured pressure some degrees before and after TDC. The reason for this is the signal to noise ratio from pressure to flywheel acceleration. Since the crank lever is zero or close to zero around TDC, the in-cylinder pressure does not affect the flywheel acceleration. Thus the acceleration reveals no information about the pressure in the TDC region. The local pressure peak before TDC is because the estimated torque trace changed sign before TDC, as discussed in Section 5.4.1. The Kalman filter also handled the division by zero at BDC (at 180° and 540°).

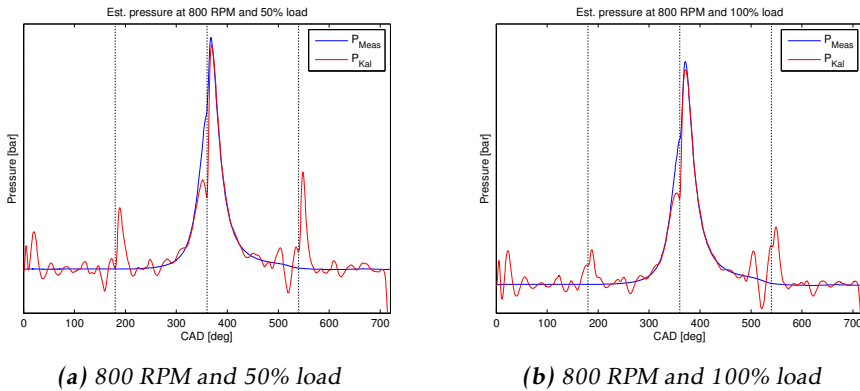


Figure 5.9: Estimated pressure from Kalman filter together with measured pressure for cylinder six at 800 RPM. The vertical dotted lines shows when the firing cylinder is in dead center.

In Figure 5.10 the estimated pressure is shown together with the measured one when the engine is running at 1000 RPM at 50% and 100% load. The oscillating behavior in the gas exchange cycle and parts of the compression and expansion stroke has increased. This is due to increased torsion in the crankshaft at engine speed 1000 RPM. A difference before TDC, compared with results from 800 RPM, is that there is no local maximum pressure peak at 1000 RPM. Analysis of the

estimated torque signal for the two load cases revealed that the estimated torque happened to be zero at TDC, and had the correct sign before and after TDC.

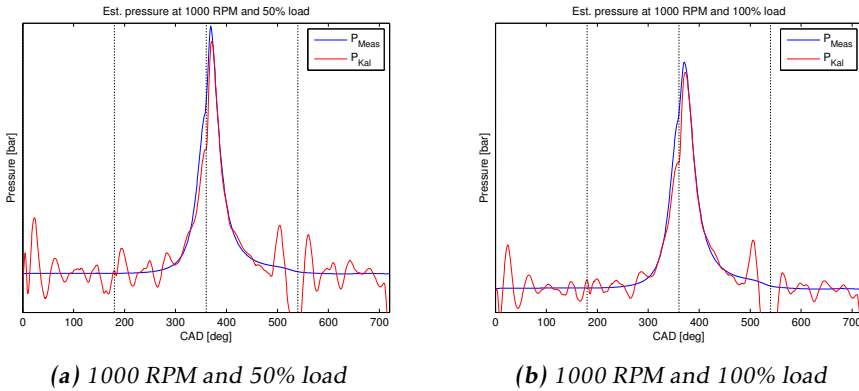


Figure 5.10: Estimated pressure from Kalman filter together with measured pressure for cylinder six at 1000 RPM. The vertical dotted lines shows when the firing cylinder is in dead center.

In Figure 5.11 the engine is running at 1600 RPM. As for the evaluated engine speeds above, two load cases are shown. As described in Section 5.2, torsion of the crankshaft has a big impact on the flywheel acceleration and thus affect the estimated torque trace from CAD-sensor data. This has clearly a huge impact on the estimated pressure as seen in the figures. The estimated pressure trace has more oscillating behavior and disturbs the compression phase that was somewhat captured at lower engine speeds. Around TDC the Kalman filter estimation does not capture the measured pressure trace as it did at lower engine speeds. The reason is that the estimated torque was negative before and after TDC.

From the figures 5.9-5.11 it is clearly seen that this pressure estimator is more sensitive to the engine speed. The estimated pressure error has still got the same percentage of error compared with the maximum pressure for the two load cases at each engine speed. With increased engine speed the crankshaft is exposed to oscillatory torques in the form of gas and mass torque, and the crankshaft twists more. The benefit of using a Kalman filter is that it uses the information in previous estimation points when a new estimate is calculated. Also it circumvents the division by zero.

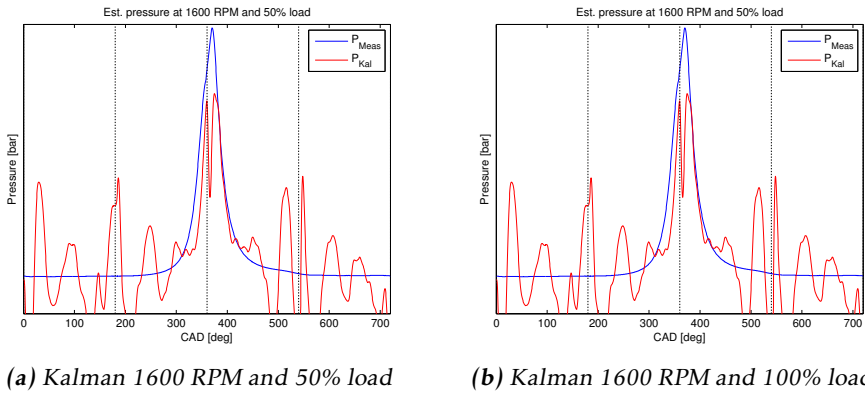


Figure 5.11: Estimated pressure from Kalman filter together with measured pressure for cylinder six at 1600 RPM. The vertical dotted lines shows when the firing cylinder is in dead center.

6

Conclusions

This thesis has investigated if it is possible to reconstruct in-cylinder pressure by performing signal processing on the CAD-sensor data together with physical modeling of a heavy-duty engine. A benefit of using the CAD-sensor is that it is a standard mounted sensor on production engines today. If a virtual pressure sensor can be designed based on this signal, no additional sensors are needed. A problem using this sensor signal is that the flywheel acceleration is perturbed by torsional effects from the crankshaft, which results in increased perturbation with increasing engine speed. The phenomenon is clearly shown in the estimated torque from CAD-sensor data in Chapter 5. By introducing a dynamic crankshaft to model these torsional effects, engine simulations confirms that torsion is one reason why estimated torque from flywheel acceleration differs from the rigid body crankshaft simulations. Further, since the flywheel acceleration is affected by many components within the engine there could still be many things that disturb the flywheel acceleration which was not investigated in this thesis. Another drawback with this method is that the signal to noise ratio when the firing cylinder is in its TDC region is zero. It is impossible to get accurate pressure data in this area based on flywheel acceleration.

The results shows some potential to capture parts of the compression and most of the expansion phase at low engine speeds. With increasing engine speed the torsional effects smears and delays information about the combustion process. In order to reconstruct this information, the signal could be filtered with the inverse function of the crankshaft model. One approach was tested but resulted in an unstable system that could not be used. Instead the separation was done with a rigid body crankshaft model. To get estimated pressure traces at higher engine speed this torsional problem needs to be solved. When reconstructing the pressure trace from the flywheel acceleration, cylinder six was chosen. This was

because it was the cylinder least affected by torsional effect. Even at 800 RPM the estimated torque trace from flywheel acceleration, when cylinder one was firing, show torsional effects. The results would probably be worse if cylinder one was chosen.

There are other sensors that captures the combustion signal around TDC, which could be combined with the investigated method for a better result. More importantly, the perturbation caused by torsional effects needs to be solved.

Bibliography

- [1] Seungeun Yu, Kyoungchan Han, Kihoon Nam, Dae Choi, and Jun Yu. Development of real-time engine control using the in-cylinder pressure signal in a diesel engine for passenger vehicle. In *SAE Technical Paper*. SAE International, 10 2013. Cited on page 1.
- [2] Frank Willems, Erik Doosje, Frank Engels, and Xander Seykens. Cylinder pressure-based control in heavy-duty egr diesel engines using a virtual heat release and emission sensor. In *SAE Technical Paper*. SAE International, 2010. Cited on page 1.
- [3] Mark C. Sellnau, Frederic A. Matekunas, Paul A. Battiston, Chen-Fang Chang, and David R. Lancaster. Cylinder-pressure-based engine control using pressure-ratio-management and low-cost non-intrusive cylinder pressure sensors. In *SAE Technical Paper*. SAE International, 03 2000. Cited on page 1.
- [4] Dirk Schiefer, Ralf Maennel, and Wesley Nardoni. Advantages of diesel engine control using in-cylinder pressure information for closed loop control. In *SAE Technical Paper*. SAE International, 03 2003. Cited on page 1.
- [5] Mikael Thor, Bo Egardt, Tomas McKelvey, and Ingemar Andersson. Using combustion net torque for estimation of combustion properties from measurements of crankshaft torque. *Control Engineering Practice*, 26:233 – 244, . ISSN 0967-0661. Cited on page 1.
- [6] Stefan Schagerberg and Tomas McKelvey. Instantaneous crankshaft torque measurements - modeling and validation. In *SAE Technical Paper*. SAE International, 03 2003. Cited on pages 2, 13, 14, 15, and 17.
- [7] M. Thor, B. Egardt, T. McKelvey, and I. Andersson. Closed-loop diesel engine combustion phasing control based on crankshaft torque measurements. *Control Engineering Practice*, 33:115–124, . ISSN 09670661. Cited on page 2.
- [8] Feilong Liu, Gehan A. J. Amaratunga, Nick Collings, and Ahmed Soliman. An experimental study on engine dynamics model based in-cylinder pres-

- sure estimation. In *SAE Technical Paper*. SAE International, 04 2012. Cited on page 2.
- [9] Stephen J. Citron, John E. O'Higgins, and Lillian Y. Chen. Cylinder by cylinder engine pressure and pressure torque waveform determination utilizing speed fluctuations. In *SAE Technical Paper*. SAE International, 02 1989. Cited on page 2.
- [10] Q.R. Butt and A.I. Bhatti. Estimation of gasoline-engine parameters using higher order sliding mode. *IEEE Transactions on Industrial Electronics*, 55 (11):3891 – 3898. Cited on page 2.
- [11] S.X. Chen and J.J. Moskwa. Application of nonlinear sliding-mode observers for cylinder pressure reconstruction. *Control Engineering Practice*, 5(8): 1115 – 1121. Cited on page 2.
- [12] I. Haskara and L. Mianzo. Real-time cylinder pressure and indicated torque estimation via second order sliding modes. volume 5, Global Dev. Technol. Center, Visteon Corp., Livonia, MI, USA. Cited on page 2.
- [13] I. Andersson and T. McKelvey. A system inversion approach on a crankshaft of an internal combustion engine. In *Proceedings of the IEEE Conference on Decision and Control*, volume 5, pages 5449–5454, Signals Department, Chalmers University of Technology. Cited on pages 2, 3, 4, 17, and 20.
- [14] Lars Eriksson and Lars Nielsen. *Modeling and control of engines and drivelines*. [Elektronisk resurs]. Automotive series. Chichester, West Sussex, U.K. : John Wiley & Sons Ltd, 2014. ISBN 9781118536193. Cited on page 3.
- [15] Serkan Kulah, Tijs Donkers, and Frank Willems. Virtual cylinder pressure sensor for transient operation in heavy-duty engines. *SAE Int. J. Engines*, 8, 04 2015. Cited on page 3.
- [16] U. Kiencke and L. Nielsen. *Automotive Control Systems: For Engine, Driveline, and Vehicle*. ISBN 9783540231394. Cited on pages 9, 10, 13, and 15.
- [17] Bengt Johansson. *Förbränningsmotorer*. Kursmaterial, 2004. Cited on page 10.
- [18] John B. Heywood. *Internal Combustion Engine Fundamentals*. MacGraw-Hill Book Company, 1988. Cited on page 15.
- [19] Neda Nickmehr. *System Identification of an Engine-load Setup Using Grey-box Model*. [Elektronisk resurs]. Linköping Studies in Science and Technology. Licentiate Thesis: 1698. Linköping : Department of Electrical Engineering, Linköping University, 2014. Cited on pages 17 and 19.
- [20] Daniel Eriksson, Lars Eriksson, Erik Frisk, and Mattias Krysander. Flywheel angular velocity model for misfire and driveline disturbance simulation. In *7th IFAC Symposium on Advances in Automotive Control*, Tokyo, Japan, 2013. Cited on page 17.



Upphovsrätt

Detta dokument hålls tillgängligt på Internet — eller dess framtida ersättare — under 25 år från publiceringsdatum under förutsättning att inga extraordinära omständigheter uppstår.

Tillgång till dokumentet innebär tillstånd för var och en att läsa, ladda ner, skriva ut enstaka kopior för enskilt bruk och att använda det oförändrat för icke-kommersiell forskning och för undervisning. Överföring av upphovsrätten vid en senare tidpunkt kan inte upphäva detta tillstånd. All annan användning av dokumentet kräver upphovsmannens medgivande. För att garantera äktheten, säkerheten och tillgängligheten finns det lösningar av teknisk och administrativ art.

Upphovsmannens ideella rätt innefattar rätt att bli nämnd som upphovsman i den omfattning som god sed kräver vid användning av dokumentet på ovan beskrivna sätt samt skydd mot att dokumentet ändras eller presenteras i sådan form eller i sådant sammanhang som är kränkande för upphovsmannens litterära eller konstnärliga anseende eller egenart.

För ytterligare information om Linköping University Electronic Press se förlagets hemsida <http://www.ep.liu.se/>

Copyright

The publishers will keep this document online on the Internet — or its possible replacement — for a period of 25 years from the date of publication barring exceptional circumstances.

The online availability of the document implies a permanent permission for anyone to read, to download, to print out single copies for his/her own use and to use it unchanged for any non-commercial research and educational purpose. Subsequent transfers of copyright cannot revoke this permission. All other uses of the document are conditional on the consent of the copyright owner. The publisher has taken technical and administrative measures to assure authenticity, security and accessibility.

According to intellectual property law the author has the right to be mentioned when his/her work is accessed as described above and to be protected against infringement.

For additional information about the Linköping University Electronic Press and its procedures for publication and for assurance of document integrity, please refer to its www home page: <http://www.ep.liu.se/>